Journal of Materials Chemistry A

ROYAL SOCIETY OF CHEMISTRY

REVIEW

View Article Online
View Journal | View Issue

Cite this: J. Mater. Chem. A, 2026, 14, 43

Leveraging battery performance through mechanically interlocked polymers

Yangju Lin, *[ab] Mingrui Liang[a] and Ahmed Eldeeb[a]

Received 19th August 2025
Accepted 3rd November 2025

DOI: 10.1039/d5ta06755c

rsc.li/materials-a

Batteries are essential energy storage devices for renewable energy sources such as solar, wind, and hydropower. The development of high-performance batteries with enhanced energy density, safety and stability often involves the development and optimization of polymeric components, including polymer electrolytes, electrode binders and coatings. Mechanically interlocked polymers (MIPs), which exhibit unique dynamics and adaptabilities due to their embedded mechanical bond motifs, have emerged as promising polymer materials. Their application in batteries has gained significant attraction in the past decade, albeit constrained by the synthetic challenges associated with these unconventional bonds. Nevertheless, integrating novel MIPs into batteries – whether as electrolytes, binders or coatings – has demonstrated considerable potential for improving battery performance. While the exploration of novel MIPs holds inherent scientific interest, their application in batteries highlights the exciting intersection between polymer design and battery technology. In this review, we summarize the progress made toward leveraging MIP materials for enhanced battery performance, aiming to inspire innovative, scalable MIP designs and underscore the significant opportunities at the interface of MIP chemistry and battery research.

[a]University of Waterloo, Department of Chemistry, Canada. E-mail: yangju.lin@uwaterloo.ca
[b]Waterloo Institute for Nanotechnology, University of Waterloo, Waterloo, Ontario N2L 3G1, Canada

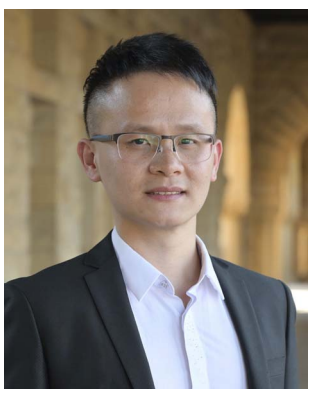

Yangju Lin

Yangju Lin is an Assistant Professor in the Department of Chemistry at the University of Waterloo, Canada. He received his BS (2012) in Chemistry and MS (2015) in Polymer Chemistry and Physics from Xiamen University, where he worked with Prof. Wengui Weng on self-healing and stress-sensing polymers. He earned his PhD (2020) under the mentorship of Prof. Stephen Craig at Duke University, focusing on the molecular engineering of stress-responsive materials. Dr Lin completed his postdoctoral research with Prof. Zhenan Bao at Stanford University, investigating the molecular design of polymer materials for batteries. His research interests span mechanistic polymer design, sustainable polymers, and polymer materials for energy storage applications.

1. Introduction

Innovation in clean and renewable energy technologies is essential to address the global impact of climate change and the impending depletion of fossil fuel resources. Batteries play a critical role in these technologies due to their importance in energy storage and release. Primarily composed of anode and cathode materials separated by electronically insulating yet ionically conductive electrolytes, batteries operate by transporting metal cations between electrodes through the electrolyte medium, driven by differences in redox potential. Concurrently, electrons flow through an external circuit, enabling energy storage during charging and controlled energy release during discharging.[1] By developing specialized high-tech components that often include novel polymeric materials,[2,3] batteries can be optimized for specific performance metrics such as high-energy density, long cycling life and high battery safety—all particularly relevant for electric vehicles and portable devices. Such polymeric components, including polymer electrolytes, electrode binders and coatings (Fig. 1a), are emerging as crucial elements of high-performance batteries. Innovation in this area remains an ongoing challenge in both basic and applied research. For example, polymer coatings have been developed to improve the cycling stability of high-energy-density lithium (Li)-metal anodes by providing robust protection, improved interfacial contact, and prevention of dendrite formation;[4,5] polymer electrolytes have been widely applied to improve battery stability and safety by overcoming the leakage

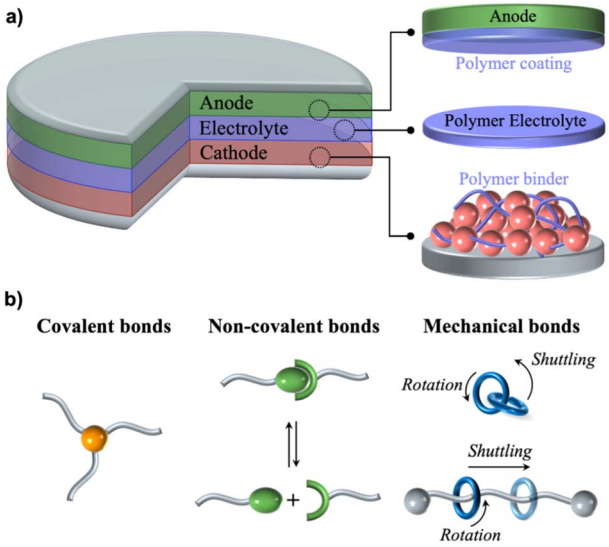

Fig. 1 (a) Typical "sandwitch" structure of batteries, with potential polymeric components indicated. (b) Schematic of conventional covalent bonds, non-covalent bonds and mechanical bonds (such as catenanes and rotaxanes) in polymer materials.

and flammability issues related to liquid electrolytes;[6,7] and polymer binders have been employed to dramatically improve electrode cycling stability by supporting mechanical integrity and enhancing capacity retention during repeated charge/discharge cycles.[8–11]

Polymer materials containing mechanical bonds,[12] also known as mechanically interlocked polymers (MIPs),[13] represent an emerging category of polymer materials. Their key components—mechanical bonds—feature both high spatial freedom (*i.e.*, rotation and shuttling) and mechanical strength comparable to covalent bonds (Fig. 1b),[14–16] endowing MIPs with combined mechanical robustness and adaptability.[17] Existing MIP designs include slide-ring materials developed by Ito *et al.*,[18] networks *via in situ* threading and crosslinking by Harada and Takashima *et al.*,[19] rotaxane crosslinked networks by Takata *et al.*,[20] and mechanical interlocked networks with dense mechanical bonds by Yan *et al.*,[12] and threaded polycatenanes and polycatenane networks by Rowan and coworkers,[21] to name a few. Many of these MIPs have recently demonstrated efficacy in enhancing battery performance, broadly attributed to their unique adaptability and mechanical resilience derived from the mechanical bonds. However, the detailed molecular mechanisms that lead to the enhanced device-level performance have yet to be fully understood.

While the development of novel MIPs remains an area of great interest, their potential applications—including use as electrolytes,[22–24] electrode coatings,[25,26] binder materials,[27] and in stretchable electronics,[28,29]—have only recently begun to be explored. A foundational challenge to advancing these technologies is the particularly arduous synthesis of MIPs, which stems from the complex design of sophisticated mechanical bond motifs. This complexity is particularly problematic when scaling production for device fabrication. For example, cyclic molecules used as hosts for mechanical bond construction often require multi-step synthesis and are typically obtained in low yields.[20,30] Nevertheless, recent efforts have demonstrated unprecedented potential for MIPs in battery applications. To this end, this minireview presents recent progress in leveraging MIPs as battery materials, aiming to inspire innovative and scalable MIP designs and highlight significant opportunities at the MIP-battery research interface.

In this review, the use of MIPs in batteries is categorized as polymer electrolytes, electrode binders, and electrode coatings. While most studies focus on polymer electrolytes, fewer studies address electrode binders and coatings. Section 2 reviews MIP applications as both solid-state and gel polymer electrolytes, with Section 2.1 highlighting how polymer structural designs influence ion-transport behaviour. Integration of these electrolytes into full batteries is discussed separately in Sections 2.2 and 2.3. Section 3 covers MIP binders specifically for silicon (Si) anodes, with no reported applications for other electrode materials to date. Section 4 introduces recent examples of MIPs as protective coatings, or artificial solid electrolyte interphases (SEIs), for high-energy-density Li-metal anodes. Finally, Section 5 discusses challenges and opportunities in leveraging MIPs as battery materials.

2. MIPs as polymer electrolytes

In contrast to conventional liquid electrolytes, which are infiltrated into polyolefin-based porous membranes to serve as ion-conducting media, polymer electrolytes function as both electrode insulators and ion conductors. Consequently, they must possess sufficient mechanical strength and ion conductivity. While tuning and enhancing polymer mechanical strength is well established in polymer science, achieving sufficient high ionic conductivity—especially in the solid state ($>10^{-4}$ S cm^{-1})—has remained a persistent challenge since their inception.[31] Nevertheless, polymer electrolytes (both solid-state and gel types) offer potential solutions to safety concerns associated with liquid electrolyte systems, such as leakage and flammability. MIPs exhibit superior mechanical strength, resilience, and unique polymer dynamic behavior owing to the molecular freedom and dynamics related to mechanical bonds. Crucially, their polymer dynamics (*e.g.*, segmental motion and diffusion) may be strongly linked to ion conduction, which poses compelling scientific questions for further exploration.

2.1 MIP polymer electrolytes

2.1.1 MIP solid-state electrolytes. Ion conduction in solvent-free solid-state polymer electrolytes can be largely dictated by the salt solvation condition and polymer segmental motion.[31,32] Generally, polymers with high segmental motion (or a low glass transition temperature, T_g) are beneficial for ion conduction.[33–37] Conversely, salt with high dissociation ability and bulky anions typically enhance ion conduction by increasing the concentration of solvated ions. Moreover, an optimal content of salt is necessary to maximize the charge carriers while avoiding excessive complexation with polymer

chains, which can restrict chain segmental motion and hinder ion conductivity.[38–40] To date, poly(ethylene oxide) (PEO)-based solid-state electrolytes remain the most ion-conductive among polymer electrolytes when formulated with an optimal salt content that effectively suppresses matrix crystallinity without excessive physical crosslinking due to dative interactions.[41–43] Similarly, enhanced segmental mobility has been found critical for improving ion conduction in solid-state PEO electrolytes. Recent computational studies indicate that abundant solvation sites and continuous ion-conducting paths within solid-state PEO electrolytes are responsible for their relatively high ionic conductivity.[44]

Cyclodextrin (CD)-PEO-based polyrotaxanes (PRs) have been the most studied MIPs for solid-state electrolytes (Fig. 2). The use of O-rich PEO chains as the axles and hydroxyl group-abundant CDs as the wheels makes these MIPs desirable as solid media for salt dissolution. Building on earlier studies of PRs, Chen and Yao *et al.*[45] first reported a crystalline pseudo-PR electrolyte consisting of α-CD-threaded PEO (α-CD-PEO) and $LiAsF_6$ salt (electrolyte denoted as polymer/ion, α-CD-PEO/Li^+) in 2014 (Fig. 3a). A short PEO chain (M_w = 2700 Da) was mixed with $LiAsF_6$ salt at a controlled ethyl oxide (EO) repeating unit to Li^+ ion ratio (EO : Li^+), then added to a saturated aqueous α-CD solution to spontaneously generate crystalline pseudo-PR electrolytes. Although the specific average number of α-CD threaded onto each PEO chain was not characterized, the obtained crystalline electrolyte was found to form ordered nanochannels as revealed by ^{13}C cross-polarization/magic angle spinning (CP/MAS) NMR spectroscopy (Fig. 3a). When the EO : Li^+ equals 2, these nanochannels provide a directional pathway and result in an ionic conductivity of ~5.6×10^{-9} S cm^{-1} at 29 °C—1.5 orders of magnitude higher than a control electrolyte comprising PEO (M_w = 2000 Da) and $LiSbF_6$ salt. Temperature-dependent conductivity analysis indicated a lower activation energy of E_a = 75.1 kJ mol^{-1} compared to the control electrolyte (E_a = 160.4 kJ mol^{-1}) (Fig. 3d). Detailed solid-state ^7Li spectra revealed five types of Li^+ species in the crystalline electrolyte, with types 1, 2 and 4 Li^+ located within the nanochannels while excluding the larger AsF_6^- anion. Notably, type 2 Li^+ acts as a transmitter, exchanging with types 1 and 4 Li^+ ions and facilitating ion transfer within the nanochannels (Fig. 3a and b). This Li^+ exchange, which is coupled to PEO chain motion within the nanochannels, enabled efficient ion conduction with an activation energy of E_a = 42.1 kJ mol^{-1}. The observed relatively low macroscopic ionic conductivity (~2.6×10^{-7} S cm^{-1} at 29 °C) was further attributed to grain boundary resistance.

To improve the PEO chain segmental motion within the nanochannels and thereby enhance ion conductivity, Chen and Yao *et al.*[46] applied β-CD as the host molecule to leverage its larger cavity size compared to α-CD (6.0 Å *vs.* 4.7 Å). The resulting β-CD-PEO/Li^+ electrolyte (β-CD : EO : Li^+ = 1.2 : 6 : 1) formed similar nanochannels and showed slightly higher ionic conductivity than the α-CD-PEO/Li^+ electrolyte (Fig. 3e). However, the activation energy for ion conduction in β-CD-PEO/Li^+ was found to be higher than that of α-CD-PEO/Li^+ (123.2 kJ mol^{-1} *vs.* 75.1 kJ mol^{-1}). They further prepared a β-CD-PEO/Na^+ electrolyte to demonstrate the applicability of these nanochannel structures. Using ^2H NMR with deuterated PEO as the axle, both β-CD-PEO/Li^+ and β-CD-PEO/Na^+ showed improved PEO chain segmental mobility compared to α-CD-PEO/Li^+. Notably, the higher ionic conductivity observed in β-CD-PEO/Na^+ relative to β-CD-PEO/Li^+ could be attributed to the lower charge density of Na^+ compared to Li^+, which reduces binding strength to O atoms and facilitates ion transport. In a subsequent study,[47] they examined the effect of chain mobility on ionic conductivity using poly (propylene oxide) (PPO, M_w = 2000 Da) polymer and PPO–PEO–PPO block copolymer (CoP, EO : PO = 1.38 : 1, M_w = 2000 Da) as the axels. Both produced crystalline electrolytes with nanochannel structures. Strikingly, the ionic conductivity of β-CD-CoP/Li^+ (β-CD : [PO + EO] : Li^+ = 1 : 2.3 : 1.23) was four orders of magnitude higher than that of β-CD-PPO/Li^+ (β-CD : PO : Li^+ = 1 : 2.4 : 1.53) at 25 °C (3.2 × 10^{-5} S cm^{-1} *vs.* 9.5 × 10^{-9} S cm^{-1}). Solid-state ^1H MAS NMR confirmed that β-CD-CoP/Li^+ has a higher segmental mobility than β-CD-PPO/Li^+. It should be noted that the MIP electrolytes investigated by Chen and Yao *et al.*[45–47] are, in fact, linear

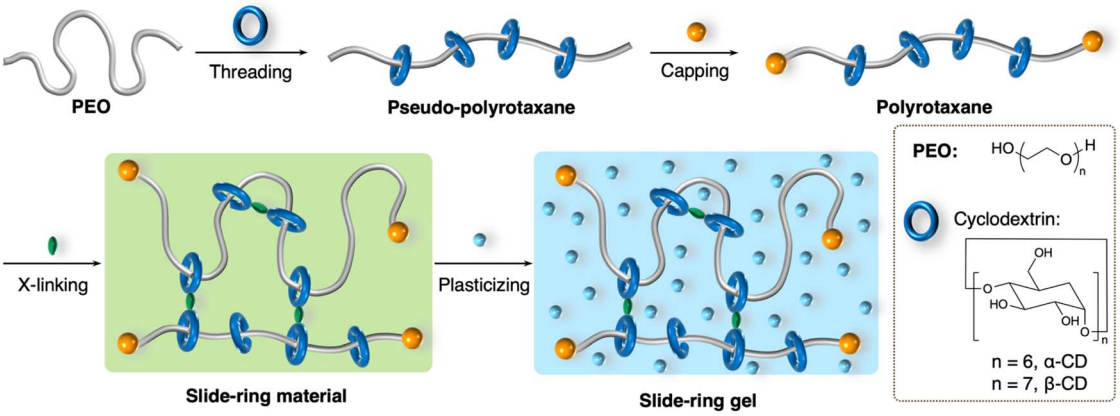

Fig. 2 Representative scheme of preparation of mechanically interlocked polymer electrolytes using PEO and CDs. The materials generated in each step—pseudo-polyrotaxane (pseudo-PR), polyrotaxane (PR), slide-ring material (SRM), and slide-ring gel (SRG)—can be adapted to polymer electrolytes by introducing various salts.

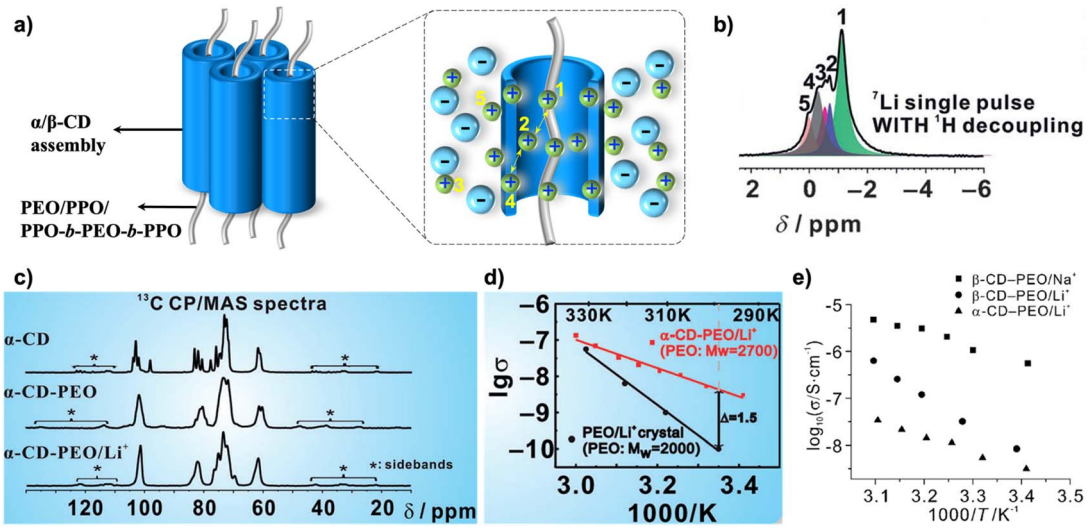

Fig. 3 (a) Pseudo-PR electrolytes consisting of nanochannels that enhance ion trnasport. (b) Solid-state ^{7}Li NMR revealing five types of Li^+ species within the pseudo-PR electrolytes. (c) ^{13}C CP/MAS spectra comparison of α-CD, α-CD-PEO and α-CD-PEO/Li^+, indicating the formation of nanochannels within the pseudo-PR electrolyte. (d) Temperature-dependent ionic conductivity of pseudo-PR electrolyte and conventional PEO/Li electrolyte, demonstrating enhanced ion transport and distinct transportation mechanisms. (e) Effect of host size and ioin speciecs on the ionic conductivity of pseudo-PR electrolytes containing nanochannels, where a larger host size enhances chain segmental motion, and presumably a lower charge density in ion species facilitates the ion transport within the nanochannels. (b–d) are reproduced from ref. 45 with persmission from Wiley, copyright 2014; (e) is reproduced from ref. 46 with persmission from Wiley, copyright 2015.

pseudo-PRs, as no chain-end capping step was performed and the threading of CDs onto the short axle polymers was relatively uncontrolled.

The mechanically trapped CDs on α-CD-PEO PRs can be crosslinked to produce crosslinked PRs, also known as slide-ring materials (SRMs) (Fig. 2), a concept first demonstrated and extensively explored by Ito and coworkers since 2001.[48] In 2017, Yokoyama and Ito *et al.*[23] fabricated a series of solid-state SRM electrolytes based on α-CD-PEO PRs. In the study, an α-CD-PEO PR consisting of a $M_w = 35\,000$ PEO and ~100 threaded α-CDs was mixed with varying $LiClO_4$ contents and further crosslinked using hexamethylene diisocyanate (HDI) (Fig. 4a). Although the exact number of crosslinking sites per chain was not provided, doubling the crosslinking sites was insufficient to suppress crystallinity. Instead, increasing the $LiClO_4$ content from 5 wt% to 15 wt% successfully eliminated crystalline domains (Fig. 4c). However, the achieved ionic conductivity remained relatively low (10^{-9}–10^{-7} S cm^{-1}) at ~80 °C. Notably, the temperature-dependent ionic conductivity exhibited a segmental motion-dictated trend at high temperatures, while showing Arrhenius-type behaviour at low temperatures—a phenomenon attributed to hydrogen-bonded CDs that limit segmental mobility. To address this limitation, they further reduced the hydrogen bonding level by reacting the hydroxyl groups on CDs using propyl isocyanate. Consequently, a degree of hydroxyl substitution on CDs of 22% improved the ionic conductivity (although still relatively low at ~10^{-7} S cm^{-1}) and enhanced mechanical ductility. Further increasing the substitution degree to 49% adversely reduced the ionic conductivity and ductility owing to hydrophobic aggregation of modified CDs. Later, Ito, Mayumi and Hashimoto *et al.*[49] sought to improve the Young's modulus of SRM electrolytes through fine-tuning PEO crystallinity and CD aggregation. An α-CD-PEO PR, composed of PEO ($M_w = 35\,000$ Da) and 9 α-CDs per PEO chain, was blended with varying Li(NTf$_2$) salt contents (EO : Li^+ = 5–33) and then crosslinked using HDI. Increasing the EO : Li^+ ratio (*i.e.*, decreasing Li(NTf$_2$) salt content) led to higher PEO crystallinity and Young's modulus without compromising maximum strain (Fig. 4d). All prepared SRM electrolytes were stretchable and exhibited strain-induced crystallization, which further enhances the electrolytes' mechanical strength (Fig. 4e). Importantly, the ionic conductivity first increased and then decreased, with a maximum value of ~10^{-5} S cm^{-1} achieved at EO : Li^+ = 10. This work demonstrated a breakthrough in overcoming the commonly known trade-offs among electrolyte modulus, ductility, and ionic conductivity.

In 2024, Seo and coworkers comprehensively investigated a series of SRM electrolytes composed of α-CD-PEO PRs with systematically varied lengths of PEO chains ($M_w = 10\,000$, 35 000, and 100 000 Da) and different numbers of threaded α-CDs per chain (35 or ~20) (Fig. 4b).[50] Overall, a higher number of α-CDs per chain led to increased formation of crystalline α-CD structures, thereby reducing α-CD mobility along the chain. These PRs were blended with $LiNO_3$ salt and further crosslinked to produce four SRM electrolytes. Comparing PRs with ~20 threaded α-CDs but different PEO chain lengths (10PRE, 35PRE and 100PRE in Fig. 4b and f), longer PEO chains provided greater α-CD sliding mobility, correlating with higher ionic conductivity. In this system, Li^+ ionic conduction appears coupled to α-CD sliding mobility. However, for the shortest PEO chain ($M_w = 10\,000$ Da), increasing the number of threaded α-CDs from ~20 to 35 (10PRE *vs.* 10DPRE) increased the ionic conductivity despite decreased α-

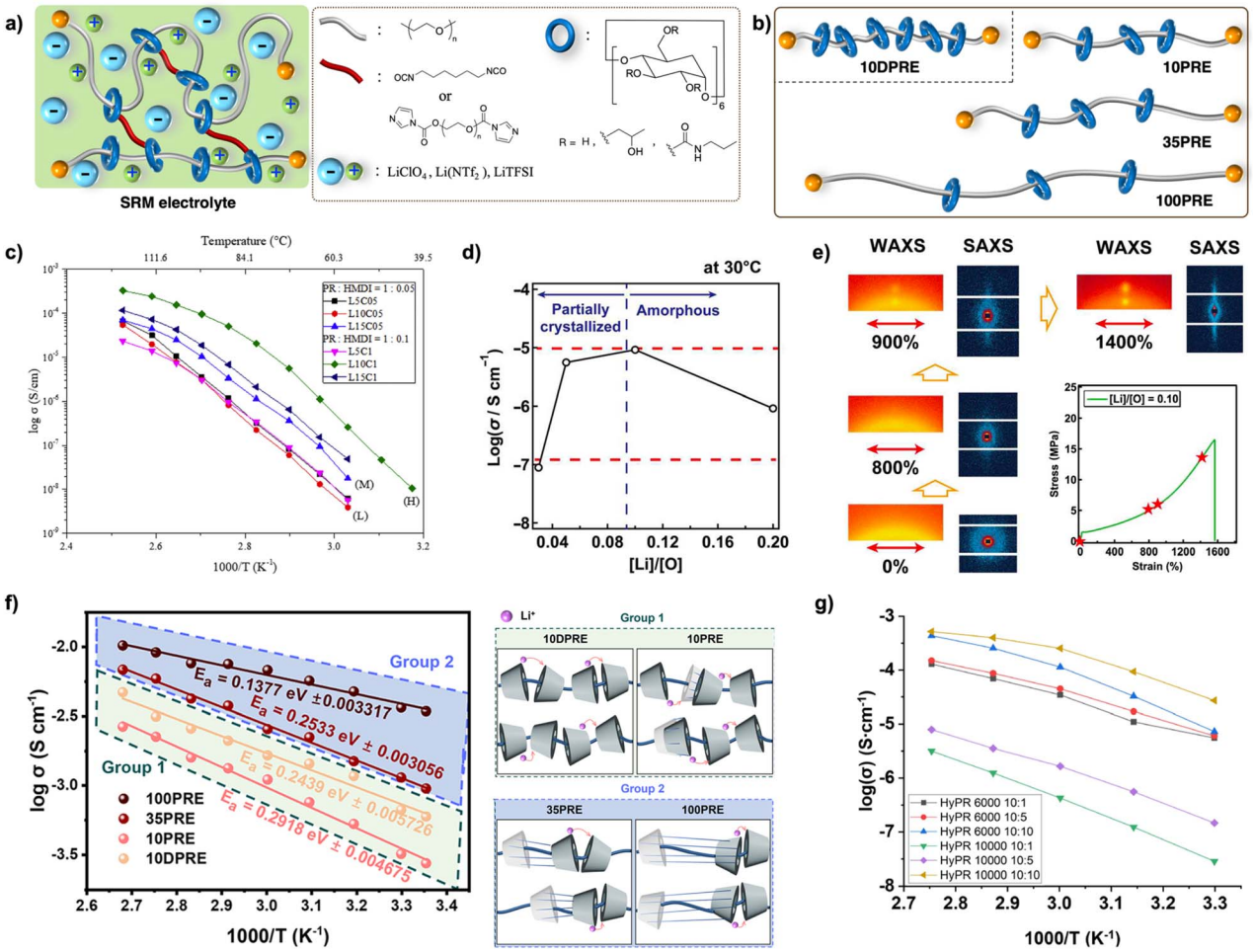

Fig. 4 (a) Compositions of SRM electrolytes in reported literature, with various crosslinkers, salts and modified CDs. (b) Tunable PRs with varied PEO axle lengths (10, 35 or 100 kDa) and wheel density (20 or 35 CDs per chian) for the fabrication of SRM electrolytes. (c) Temperature-dependent ionic conductivity of SRM electrolytes with various salt contents and crosslinking densities. L*x*C*y*: $x = 5$, 10, 15 wt% $Li(NTf)_2$ salt; $y = 0.5$ or 1 for 5 and 10 mol% HDI crosslinker, respectively. (d) Evolution of ionic conductivity over Li^+/EO (or [Li]/[O]) ratio in the SRM electrolytes. (e) WAX and SAXS studies of crystallinity in a SRM electrolyte under different strains. (f) Impact of PEO chain length and CD density in PR on the ionic conductivity of fabricated SRM electrolytes. (g) Effects of the chain length of macrolinker and crosslinkng density on the ionic conductivity of SRM electrolytes. For the legends, HyPR6000/10 000 refers to the use of hydroxypropyl modified CDs and 6/10 kDa macrolinker, and the following ratio indicates the PR and macrolinker weight ratios. (c) is reproduced from ref. 23 with permission form Elsevier, copyright 2018; (d and e) are reproduced from ref. 49 with permission form The American Association for the Advancement of Science, copyright 2024; (f) is reproduced from ref. 50 with permission form American Chemical Society, copyright 2024; and (g) is reproduced from ref. 51 with permission form American Chemical Society, copyright 2024.

CD sliding mobility. ^{7}Li NMR studies attributed this effect to enhanced $LiNO_3$ dissociation related to higher α-CD content. As such, Li^+ conduction in PRs with high α-CD content was postulated to occur through hopping along the threaded and aligned α-CDs. The SRM electrolytes design demonstrated significant advantages over controls comprising PEO and physically blended α-CDs, with ionic conductivity enhanced by a factor of ~330. Notably, an impressive ionic conductivity of 3.4×10^{-3} S cm^{-1} at 25 °C was reported using the PEO with $M_w = 100\,000$ Da and ~20 threaded α-CDs.

Yin and You *et al.*[51] also reported SRM electrolytes employing α-CD-PEO PRs combined with PEO macromolecular crosslinkers instead of small-molecule crosslinkers. A PEO with $M_w =$ 35 000 Da was used to prepare a PR containing ~100 threaded α-CDs, which were further functionalized with hydroxypropyl groups before crosslinking with modified PEO macrolinkers (M_w = 6000 or 10 000 Da). At 15 wt% LiTFSI content, the as-prepared SRM electrolytes showed substantially reduced α-CD crystallinity and slightly increased PEO crystallinity with increasing amounts of PEO macrolinkers, offering improved electrolyte ductility. Similarly, longer PEO macrolinkers (10 000 *vs.* 6000 Da) led to reduced α-CD crystallinity but slightly increased PEO crystallinity. Overall, increased macrolinker content or longer macrolinker length resulted in SRM electrolytes with higher polymer segmental mobility and corresponding enhanced ionic conductivity (Fig. 4g). All prepared electrolytes showed good thermal stability >150 °C. The α-CD crystalline domains, which govern chain segmental mobility

and ionic conductivity, could be eliminated by heat treatment. As a result, all SRM electrolytes exhibited improved ionic conductivities, with a maximum conductivity of 2.7×10^{-5} S cm^{-1} at 30 °C. Pursuing further improvements, a longer PEO macrolinker with $M_w = 35\,000$ was applied to fabricate SRM electrolyte.[52] Despite an increase in PEO crystallinity, the α-CD crystallinity responsible for chain segmental mobility was successfully suppressed as the macrolinker length increased from $M_w = 6000$ Da to $M_w = 35\,000$ Da. Overall, the SRM electrolyte with a PEO macrolinker of $M_w = 10\,000$ Da provided the optimal ionic conductivity of 7.05×10^{-5} S cm^{-1} at 30 °C.

2.1.2 MIP gel electrolytes. The addition of plasticizers to a polymer electrolyte enhances chain segmental mobility and modifies ion conduction mechanisms, resulting in substantial improvements in ionic conductivity (Fig. 5). Plasticizers act as "molecular lubricants", disrupting interchain interactions such as hydrogen bonding and van der Waals forces, while simultaneously increasing the free volume within the polymer matrix. This combination remarkably enhances chain segmental mobility, facilitating ion transport. Meanwhile, plasticizers solvate the salt and enable ions to transport more readily along the liquid path within the polymer matrix, effectively lowering activation energy for ion transport.[53–55] However, these benefits come with trade-offs including reduced mechanical strength and potential safety risks due to the flammability of added plasticizer. To worth mentioning, the polymer osmotic pressure allows the plasticizer to be retained within the polymer matrix, mitigating the leakage of liquid plasticizer.

Slide-ring gels (SRGs) developed by Okumura and Ito[48] exhibited excellent mechanical ductility owing to the adaptive shuttling of α-CDs under external mechanical load. Consequently, SRGs offer a promising approach for the fabrication of gel electrolytes that address the trade-off between ionic conductivity and mechanical strength. Building on previous studies on SRGs, Shimomura and Ito *et al.*[56] investigated the conductivity and mechanical strength of α-CDs-PEO-based SRG electrolytes swollen with propylene carbonate and LiTFSI salt. A PR composed of a PEO with $M_w = 35\,000$ Da and ~100 threaded α-CDs was crosslinked with various amounts of divinyl sulfone crosslinker. Due to the poor affinity of propylene carbonate toward α-CDs, the SRM could not be swollen to form an SRG electrolyte. However, after 28% or 74% methylation of α-CDs' hydroxyl groups, SRMs could be successfully swollen (swelling ratios of 107–108%) to give SRG electrolytes exhibiting high ionic conductivity of $2.2–3.9 \times 10^{-3}$ S cm^{-1} at 25 °C. Slightly reducing crosslinking density moderately improved ionic conductivity while slightly reducing the modulus. Notably, the activation energy for ion conduction was comparable to that of a pure electrolyte solution, suggesting a similar ion conduction mechanism to that of a liquid electrolyte. Alternatively, Shimomura and Ito *et al.*[57] utilized a series of imidazolium-based ionic liquids to prepare the SRG electrolyte. α-CDs with and without 50% hydroxypropyl substitution were applied to fabricate the SRG electrolytes, which swelled slowly in the ionic liquids over a week. Obtained SRG electrolytes showed Young's moduli of 15–30 kPa and high ionic conductivities of $1.66–3.18 \times 10^{-3}$ S cm^{-1} at 20 °C, with 1-ethyl-3-methylimidazolium ethyl sulfate providing the highest ionic conductivity. Further addition of LiTFSI salt to the ionic liquid improved the ionic conductivity ($2.66–4.31 \times 10^{-3}$ S cm^{-1} at 30 °C) and mechanical properties (8.4–60.5 kPa Young's modulus), rendering the SRG electrolytes suitable for Li-ion batteries (Table 1).[22]

Shimomura and Ito *et al.*[58] further expanded this SRG system to gel electrolytes containing Mg^{2+} ion, using 0.5 mol L^{-1} Mg(TFSI)$_2$ in diethylene glycol dimethyl ether (diglyme; G2), triethylene glycol dimethyl ether (triglyme; G3), or tetraethylene glycol dimethyl ether (tetraglyme; G4) as swelling liquid electrolytes. Interestingly, swelling behaviour was highly dependent on the glyme solvent: G4 showed no swelling, while G2 and G3 reached swelling equilibrium in one and three weeks, respectively. It was postulated that exclusive coordination of Mg^{2+} with G4 prevents its interaction with α-CD and PEO chains, inhibiting the network swelling property. G3 provided the highest swelling ratio and the greatest electrolyte uptake and was therefore systematically evaluated by varying crosslinking density. Increasing crosslinking density improved modulus but reduced ductility and ionic conductivity. The ion conduction was found to follow a segmental motion-coupled ion transportation mechanism, with an optimized ionic conductivity of 1.73×10^{-3} S cm^{-1} at 25 °C.

2.2 MIP solid-state electrolytes for batteries

Like other solid-state polymer electrolytes, the relatively low ionic conductivity in MIP solid-state electrolytes remains a long-standing challenge for their application in full batteries. Initial attempts have successfully demonstrated their application potential at elevated temperatures. In 2018, Brunklaus, Winter and colleagues prepared a series of pseudo-PR electrolytes using

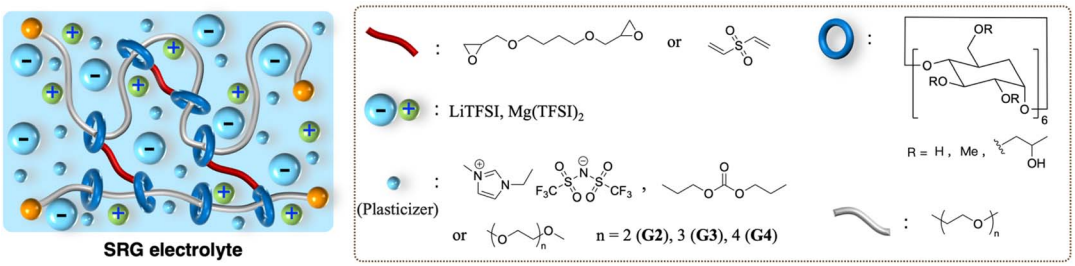

Fig. 5 Schematic compositions of SRG electrolytes in reported literature, including various crosslinkers, salts, modified CDs and plasticizers.

Table 1 Summary of MIP polymer electrolytes with corresponding electrochemical and mechanical properties

Electrolyte type	[a]Polymer design	Salt (and [b]plasticizer)	σ (S cm^{-1})	E_a (kJ mol^{-1})	t_+	[c]Mechanical property (σ_{max}, ε_{max} and E)	Ref.
Solid-state	α-CD-PEO (pseudo-PR)	$LiAsF_6$	5.6×10^{-9} (30 °C)	75.1	NA	NA NA NA	45
	β-CD-PEO (pseudo-PR)	$LiAsF_6$	8.3×10^{-9} (25 °C)	123.2	NA	NA NA NA	46
	β-CD-PEO (pseudo-PR)	$NaAsF_6$	5.5×10^{-7} (25 °C)	58.2	NA	NA NA NA	46
	β-CD-PEO-*co*-PPO (pseudo-PR)	$LiAsF_6$	3.2×10^{-5} (25 °C)	NA	NA	NA NA NA	47
	β-CD-PPO (pseudo-PR)	$LiAsF_6$	9.5×10^{-9} (25 °C)	NA	NA	NA NA NA	47
	HyPr-α-CD-PEO + HDI (SRM)	$LiClO_4$	$\sim 10^{-7}$ (60 °C)	23.2	NA	16.6 MPa 200% 570 MPa	47
	α-CD-PEO + HDI (SRM)	$Li(NTf_2)$	$\sim 10^{-5}$ (30 °C)	9.4	NA	15.6 MPa 1600% ~10 MPa	49
	α-CD-PEO + MDI and HDI (SRM)	$LiNO_3$	3.4×10^{-3} (25 °C)	13.3	0.63	NA NA NA	50
	HyPr-α-CD-PEO + PEO macrolinker (SRM)	LiTFSI	2.7×10^{-5} (30 °C)	NA	NA	4.9 MPa 552% ~12.5 MPa	51
Gel	Me-α-CD-PEO + divinyl sulfone (SRG)	LiTFSI + PC	2.9×10^{-3} (25 °C)	6.8	NA	NA [d]51.5% 14.8 kPa	56
	HyPr-α-CDs-PEO + diglycidyl ether (SRG)	EMIES	$1.7–3.2 \times 10^{-3}$ (20 °C)	NA	NA	NA NA 15–30 kPa	57
	HyPr-α-CDs-PEO + divinyl sulfone (SRG)	LiTFSI + EMITFSI	$2.66–4.31 \times 10^{-3}$ (30 °C)	2.8–3.0	NA	NA NA 8.4–60.5 kPa	22
	α-CDs-PEO + divinyl sulfone (SRG)	$Mg(TFSI)_2$ + G3	1.73×10^{-3} (25 °C)	1.35	NA	0.05 MPa 300% 20 kPa	58

[a] Indicated with host molecule and guest polymer chain. HyPr-α-CD refers to hydroxypropyl modified α-CD; Me-α-CD denotes methylated α-CDs; HDI represents hexamethylene diisocyanate, and MDI means methylene diphenyl diisocyanate. [b] PC indicates propylene carbonate; EMIES means 1-ethyl-3-methylimidazolium ethyl sulfate, and EMITFSI is 1-ethyl-3-methylimidazolium bis(trifluoromethylsulfonyl)imide; G3 is triethylene glycol dimethyl ether. [c] σ_{max} refers to maximum tensile stress, ε_{max} indicates maximum tensile strain, and E means Young's modulus. [d] Compression strain.

a short chain PEO ($M_w = 2000$) and both pristine and methylated α-, β-, γ-CDs (Fig. 6a).[59] The prepared electrolytes had a CD : EO ratio of 1 : 2.8 and exhibited nanochannel structures similar to those reported by Chen and Yao *et al.*[45–47] after being blended with LiTFSI salt at an EO : Li ratio of 5 : 1. Interestingly, all methylated CDs exhibited higher ionic conductivity than the pristine counterparts, attributed to their less rigid structures due to the absence of hydrogen bonds between CDs. Notably, the ionic conductivity followed the trend α-CDs < β-CDs < γ-CD, correlating with cavity size-dependent PEO chain segmental mobility (Fig. 6b). Consequently, the methylated γ-CD electrolyte showed an ionic conductivity of $\sim 10^{-4}$ S cm^{-1} at 100 °C, with a transport number of $t_+ \sim 0.34$. This electrolyte was further demonstrated to outperform a control PEO/LiTFSI electrolyte in full battery tests (Fig. 6c). Brunklaus and Winter *et al.*[24] further investigated CD-PEO based PR electrolytes containing polycaprolactone (PCL) grafted CDs (Fig. 6d), following a preparation method previously reported by Kato *et al.*[60] A similar low molecular weight PEO ($M_w = 3000$) was used to prepare chain-end capped PR. Although the CD coverage ratio was

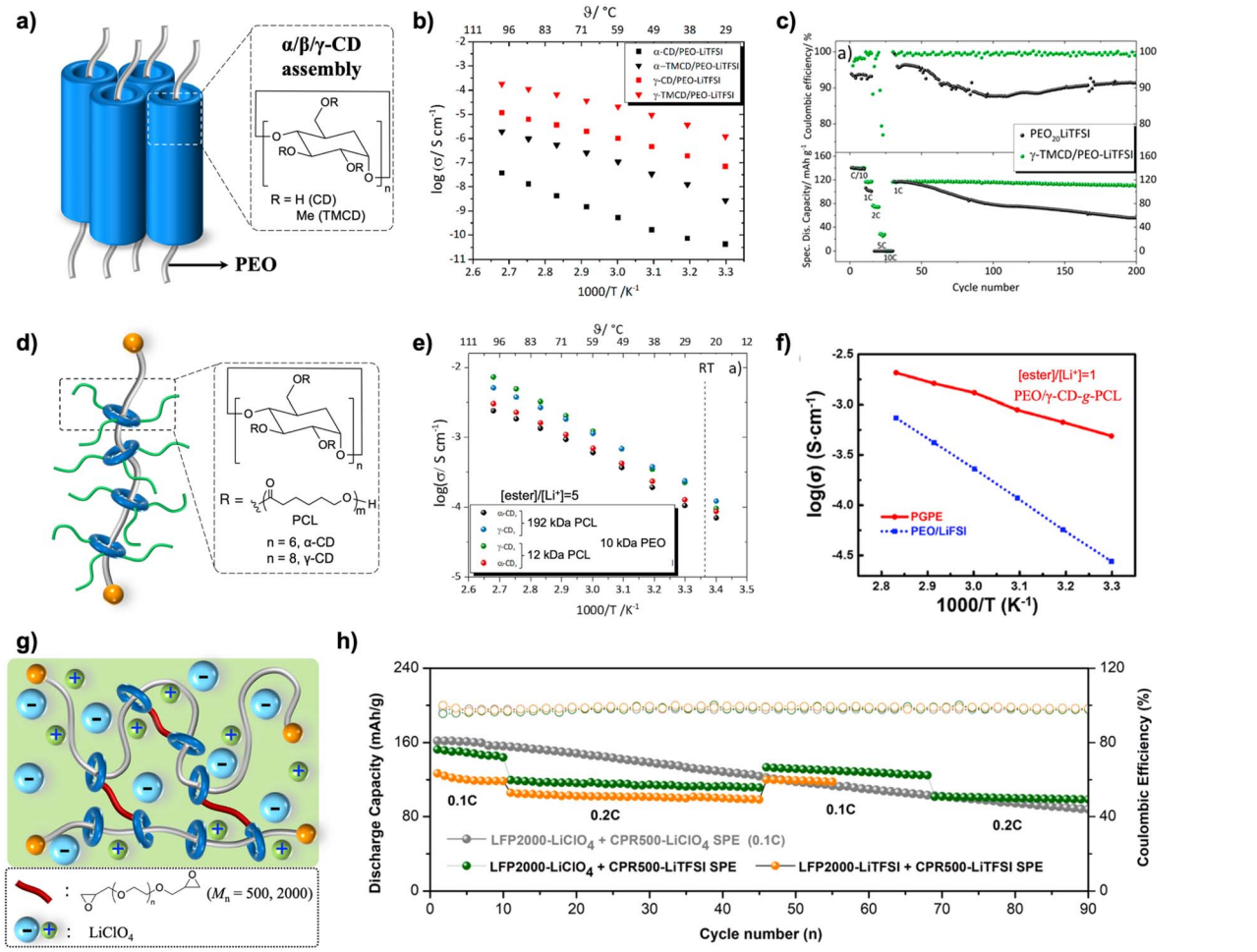

Fig. 6 (a) Pseudo-PR electrolytes consisting of different CDs and LiTSI salt show nanochannel structuctures, and their corresponsing temperature-dependent ionic conductivity properties are shown in (b). (c) The use of a pseudo-PR electrolyte comprising methylated γ-CD and PEO presents improved cycling stability compared with a conventional PEO/LiTFSI electrolyte. (d) Schematic PR electrolytes containing PCL-grafted CD wheels. (e) The length effect of grafted PCL (12 or 192 kDa) and CD species (α- or γ-CD) on the PR electrolyte ionic conductivities. (f) Ionic conductivity of a "polymer-in-salt" electrolyte containing PCL-grafted-CD-PEO PR (38 wt%) and LiFSI salt (62 wt%). (g) SRM electrolyte with PEO macrolinkers and (h) their performance in an LFP||Li full battery (CPR500 refers to SRM electrolyte crosslinked using a 500 Da PEO macrolinker). (b and c) are reproduced from ref. 59 with permission form American Chemical Society, copyright 2018, (e) is reproduced from ref. 24 with permission from Elsevier, copyright 2019, (f) is reproduced from ref. 62 with permission form American Chemical Society, copyright 2019, and (h) is reproduced from ref. 62 with permission from Elsevier, copyright 2024.

unspecified, the number of grafted caprolactone units per CD was varied from 48 to 103. The use of γ-CD grafted with long PCL chains and at a LiTFSI salt content of $[ester]:[Li^+] = 5:1$ provided optimal ionic conductivity, with impressive values $>10^{-4}$ S cm^{-1} at room temperature and 10^{-3} S cm^{-1} at 60 °C (Fig. 6e). A Li||Li symmetric cell employing this PR electrolyte exhibited stable cycling for >600 cycles under a current of 0.1 mA cm^{-2} at both 40 and 60 °C (Table 2).

The concept of polymer-in-salt,[61] in which salt is the major component (>50 wt%), has been shown to yield relatively high ionic conductivity in solid-state electrolytes. A similar PCL-grafted γ-CD-PEO PR (38 wt%) and LiFSI (62 wt%) were mixed and infiltrated into a porous polyimide film to prepare the PR-in-salt electrolyte.[62] The obtained electrolyte exhibited a high ionic conductivity of 4.89×10^{-4} S cm^{-1} at 30 °C (Fig. 6f) and demonstrated superior cycling in Li||Li symmetric cells and NCM811||Li full cells compared to a PEO/LiFSI counterpart. The improved battery performance was further revealed by transmission electron microscopy (TEM) and X-ray photoelectron spectroscopy (XPS) studies of the NMC811 cathode after cycling, which showed that a smooth, uniform, continuous, and dense CEI layer formed from the PR-in-salt electrolyte prevented transition metal dissolution and additional side reactions.

In another study, Gohy and Jia *et al.*[63] prepared several SRM electrolytes composed of α-CD-PEO PR (PEO M_w = 35 000 Da with ~100 threaded α-CDs), PEO crosslinker, and $LiClO_4$ salt (Fig. 6g). By tuning the PEO crosslinker length (M_w = 500 or 2000 Da) and $LiClO_4$ salt content (EO : Li = 8 : 1–20 : 1), an optimal ionic conductivity of 7.25×10^{-4} S cm^{-1} at 60 °C was achieved using a PEO crosslinker with M_w = 500 and $EO:Li^+ = 10:1$. Consequently, this optimized SRM electrolyte was demonstrated in both Li||Li symmetric cells and LFP||Li full

Table 2 Application of MIP electrolytes in various of full batteries

Electrolyte type	[a]Polymer design	[b]Salt (and plasticizer)	σ (S cm^{-1})	t_+	LSV onset *vs.* Li/Li$^+$	[c]Full battery	Cycling stability	Ref.
Solid-state	γ-CD-PEO (pseudo-PR)	LiTFSI	~10^{-4} (100 °C)	0.34 (70 °C)	NA	Li‖LFP (1.2 mg cm^{-2}) (2.5–3.8 V)	95% retention after 200 cycles at 1C, average CE = 99.4% (60 °C)	59
	PCL-*g*-α-CD-PEO (PR polymer-in-salt)	LiFSI	4.89×10^{-4} (30 °C)	0.64 (30 °C)	4.7 V (10 mV s^{-1}, 30 °C)	Li‖NCM811 (3–4 mg cm^{-2}) (3.0–4.3 V)	80% retention after 100 cycles and 68% retention after 150 cycles at 0.2C, average CE = 99% (30 °C)	62
	α-CD-PEO + PEO linker (SRM)	$LiClO_4$	7.25×10^{-4} (60 °C)	0.54 (60 °C)	> 4.8 V (1 mV s^{-1}, 60 °C)	Li‖LFP (1.0 mg cm^{-2}) (3.0–3.8 V)	56% retention after 90 cycles at 0.1C (60 °C)	63
	18C6-PEO + HDI (crosslinked PR)	LiTFSI	3.48×10^{-4} (25 °C)	0.41 (25 °C)	> 4.8 V (1 mV s^{-1}, 25 °C)	Li‖LFP (2–3 mg cm^{-2}) (2.5–4.0 V)	96.5% retention after 250 cycles at 0.5C (25 °C)	64
Gel	α-CD-PEO + PVDF-HFP (pseudo-PR composite)	$LiPF_6$ + EC/EMC/DEC	1.73×10^{-4} (25 °C)	0.69 (25 °C)	5.25 V (1 mV s^{-1}, 25 °C)	Li‖LFP (1.5–1.7 mg cm^{-2}) (2.5–4.0 V)	No obvious decay after 40 cycles at 1C (25 °C 55 °C or 80 °C)	67
						Li‖NMC532 (loading NA)	86% retention after 300 cycles at 0.5C rate (25 °C)	67
	α-CD-PEO + PVDF-HFP (pseudo-PR composite)	LiTFSI + DDN	8.3×10^{-4} (25 °C)	0.51 (25 °C)	> 4.5 V (1 mV s^{-1}, 25 °C)	Li‖LFP (loading NA) (2.5–3.8 V)	99.02% after 100 cycles and 78.8% after 500 cycles at 1C (25 °C)	68
	α-CD-PEO + PAM (pseudo-PR composite)	$Zn(OTf)_2$ + H_2O	22.4×10^{-3} (25 °C)	0.92 (25 °C)	NA	Zn‖La–V_2O_5 (1.0 mg cm^{-2}) (0.4–1.6 V)	90.2% retention after 3500 cycles at 5 A g^{-1} (25 °C)	69
	α-CD-PEO + HDI (SRG)	$LiNO_3$ + DMSO	5.93×10^{-3} (25 °C)	0.71 (25 °C)	4.7 V (10 mV s^{-1}, 25 °C)	Li‖LFP (2.1 mg cm^{-2}) (2.5–4.0 V)	91.2% retention after 100 cycles at 0.1C, 98.6% CE (25 °C)	70
	α-CD-PEO + PnBA + PEO macrolinker (SRG)	$LiNO_3$ + DMSO	2.8×10^{-3} (25 °C)	0.61 (25 °C)	4.8 V (10 mV s^{-1}, 25 °C)	Li‖O_2 (500 mAh g^{-1} limit)	>300 cycles at 0.2C rate and 200 cycles at 1C rate (25 °C)	71
	α-CD-PEO + PEO macrolinker (SRG)	LiTFSI + DDN	1.73×10^{-3} (30 °C)	0.71 (30 °C)	4.7 V (1 mV s^{-1}, 25 °C)	Li‖LFP (2.4–2.6 mg cm^{-2}) (2.8–4.0 V)	89.6% retention after 1000 cycles at 1C, 96.4% retention after 250 cycles at 5C (25 °C)	71
	α-CD-PEO + tetra-arm linker (SRG)	LiTFSI + EMIMTFSI	2.21×10^{-3} (20 °C)	0.45 (20 °C)	4.6 V	Li‖NMC622 (1.1 mg cm^{-2})	92% retention after 300 cycles at 0.1C (20 °C)	73

[a] PCL-*g*-α-CD means PCL-grafted α-CD, 18C6 refers to 18-crown-6-ether, and HDI denotes hexamethylene diisocyanate. [b] EC, EMC, and DEC refer to ethylene carbonate, ethyl methyl carbonate, and diethyl carbonate, respectively; DDN electrolyte: LiTFSI dissolved in a 1 : 1 (v/v) mixture of 1,3-dioxolane (DOL) and 1,2-dimethoxyethane (DME), with a 1 wt% addition of $LiNO_3$; EMIMTFSI refers to 1-ethyl-3-methylimidazolium bis(trifluoromethylsulfonyl)imide. [c] Paired cathode with indicated areal loading and cut-off voltage for battery cycling.

cells to provide stable cycling at 60 °C (Fig. 6h). Notably, the LFP cathode was fabricated using 40 wt% SRM electrolyte as the binder or catholyte.

Beyond CD-PEO-based PR electrolytes, Yu, Guo, and Tang *et al.*[64] designed a chain-end crosslinked PR electrolyte containing threaded 18-crown-6-ether rings on the PEO network strands (Fig. 7a). This novel MIP electrolyte was prepared through *in situ* threading and crosslinking of PEO chains in the presence of 18-crown-6-ether rings. Although the number of threaded crown ether rings was not specified, the obtained electrolyte exhibited an impressive ionic conductivity of 3.48×10^{-4} S cm^{-1} at room temperature. This electrolyte was further used to demonstrate stable cycling of a Li‖Li symmetric cell and an LFP‖Li full cell at 25 °C (Fig. 7b).

2.3 MIP gel electrolytes for batteries

The enhanced ionic conductivity in MIP gel electrolytes enables their practical application in batteries, albeit at the cost of compromised mechanical strength and thermal stability. Introducing external particles into the gel electrolyte to form a polymer composite gel electrolyte enhances the mechanical strength and thermal stability of gel electrolytes. Notably, the electronic states and physicochemical properties—including redox stability, dielectric constant, polymer crystallinity and relaxation dynamics, ionic conductivity, and surface energy—are indeed simultaneously modified when forming polymer composites. This collective alteration substantially influences the overall electrochemical performance.[65,66] A similar strategy has also been explored in the context of MIP gel electrolytes. Tong *et al.*[67] performed a one-pot preparation of a pseudo-PR composite consisting of PEO (M_w = 20 000), α-CD (~32 α-CDs per PEO chain), poly(vinylidene fluoride-*co*-hexafluoropropylene) (PVDF-HFP), and liquid PEO (M_w = 400) (Fig. 8a). This composite was subsequently immersed in an electrolyte solution containing 1 mol L^{-1} $LiPF_6$ and an equal-volume mixture of ethylene carbonate (EC), ethyl methyl

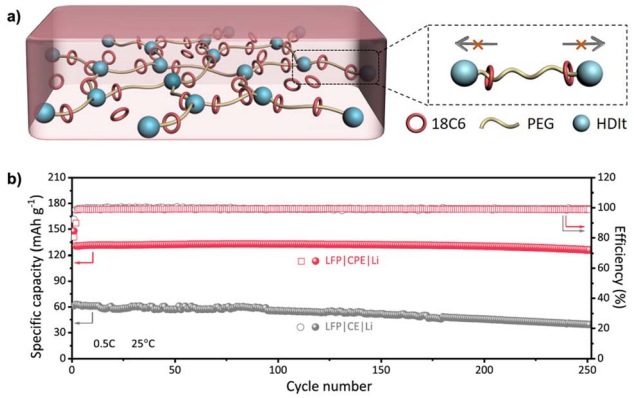

Fig. 7 (a) Schematic of a chain-end crosslinked PR network electrolyte (CPE) containing interlocked crown ethers, and (b) its use in an LFP||Li full battery showing a stable and improved cycling at 25 °C, compared with a non-interlocked counterpart CE. Reproduced from ref. 64 with permission form American Chemical Society, copyright 2023.

carbonate (EMC), and dimethyl carbonate (DEC) (volume ratio 1 : 1 : 1). Although the precise plasticizer fraction was not characterized, the composite gel electrolyte with a PEO : PVDF-HFP weight ratio of 1 : 2 provided an ionic conductivity of 1.73×10^{-4} S cm^{-1} at room temperature. This composite exhibited high thermal stability with <20% shrinkage at 200 °C, significantly outperforming a commercial Celgard 2400 membrane (Fig. 8b). Cycling in a Li||Li symmetric cell and an LFP|Li full cell demonstrated promising stability (Fig. 8c). Zhu and Tong *et al.*[68] further incorporated nano-Al_2O_3 particles to the gel electrolyte to reinforce both ionic conductivity and mechanical strength. The modified composite electrolyte exhibited an improved ionic conductivity of 8.30×10^{-4} S cm^{-1}, a Li^+ transfer number of 0.51, and a tensile strength of 17.12 MPa. This enhancement is attributed to multiple molecular interactions, including PEO–Li^+, Al_2O_3–Li^+ and F–Li^+ interactions. The new composite gel electrolyte exhibited improved cycling performance in an LFP||Li (LFP loading unspecified) full cell compared with the counterpart lacking nano-Al_2O_3.

The pseudo-PR gel electrolyte was also applied in flexible zinc-ion batteries, which possess high energy density, low cost, and intrinsic safety. Sun, Zhang and Miao *et al.*[69] prepared an α-CD-PEO pseudo-PR and subjected it to the *in situ* polymerization of polyacrylamide (PAM) in the presence of $Zn(OTf)_2$ salt, yielding a α-CD-PEO/PAM pseudo-PR hydrogel electrolyte containing both free and threaded α-CDs (Fig. 8a). This hydrogel electrolyte exhibited higher mechanical toughness and adhesion compared to the PAM hydrogel electrolyte (Fig. 8d). Impressively, a high room-temperature ionic conductivity of 22.4×10^{-3} S cm^{-1} with an outstanding Li^+ transfer number of 0.923 was achieved at 60 wt% water content, substantially outperforming the PAM electrolyte (9.4×10^{-3} S cm^{-1}) with the same water content. The use of this pseudo-PR hydrogel electrolyte in a La–V_2O_5||Zn (~1.0 mg cm^{-2} La–V_2O_5 loading) coin cell demonstrated 90.2% capacity retention after 3500 cycles at 5 A g^{-1} current density (Fig. 8e). Additionally, the mechanically tough hydrogel electrolyte enabled flexible zinc-ion batteries resilient to various mechanical load such as bending, cutting, and puncturing.

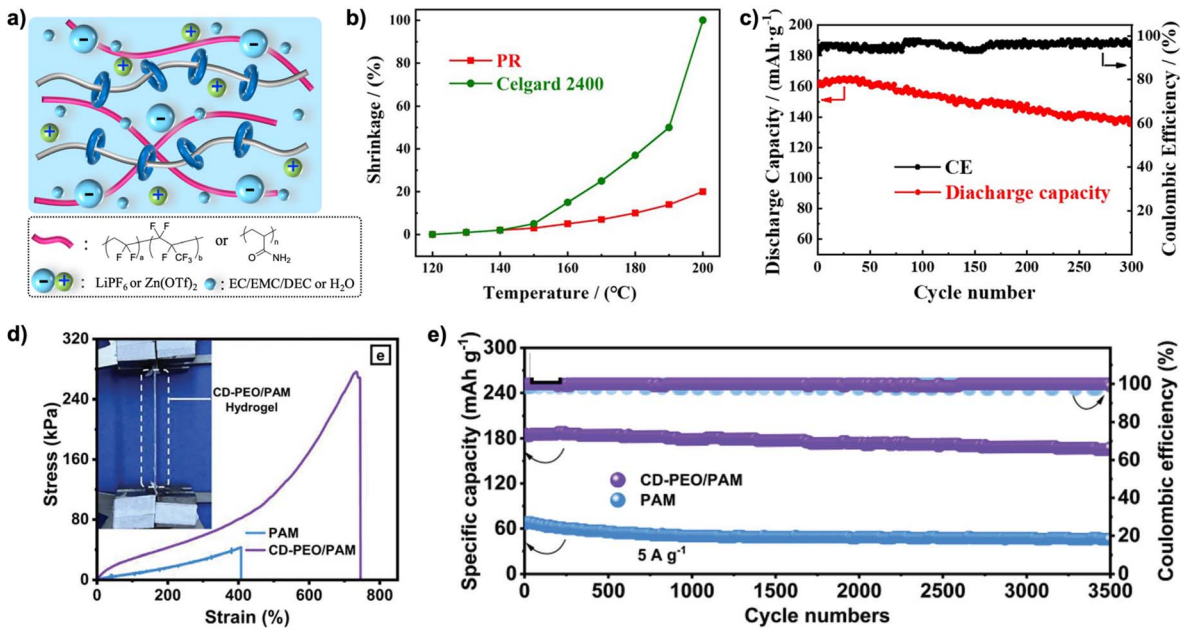

Fig. 8 (a) Composite gel electrolyte consisting of pseudo-PR and PVDF-HFP or PAM. (b) A pseudo-PR composite gel electrolyte exhibited higher thermal stability than a commercial Celgard 2400 membrane, and (c) its use in an NMC532||Li full battery enabled 86% capacity retention after 300 cycles at 0.5C. A CD-PEO/PAM composite electrolyte showed higher (d) mechanical toughness and (e) cycling capacity in a La–V_2O_5||Zn battery than the PAM gel electrolyte. (b and c) are reproduced from ref. 68 with permission from Springer, copyright 2022. (d and e) are reproduced from ref. 69 with permission from Wiley, copyright 2023.

Compared with (pseudo-)PR gel electrolytes, SRG electrolytes possess improved dimensional stability. Aiming to simultaneously improve the ionic conductivity and mechanical strength of gel electrolytes, Kim and Seo *et al.*[70] fabricated an SRG electrolyte based on α-CD-PEO PR (with PEO $M_w = 10\,000$ Da) and a HDI crosslinker (Fig. 9a). The glucose unit of α-CD was found to provide stronger solvation of $LiNO_3$ than LiTFSI and $LiClO_4$, owing to strong binding between hydroxyl groups and NO_3^- anion (Fig. 9b). Accordingly, a highly elastic SRG electrolyte containing $LiNO_3$ salt and 37 wt% DMSO exhibited a high ionic conductivity of 5.93×10^{-3} S cm^{-1} at 25 °C, with a Li^+ transfer number of 0.71 and mechanical toughness of 14.3 MJ m^{-3}. The high ionic conductivity was attributed to the high free motion of threaded α-CDs, including sliding and rotation. The utilization of the SRG electrolyte was further demonstrated in an LFP||Li full cell at 25 °C (Fig. 9c). To enable the use of SRG electrolyte in Li–oxygen (O_2) batteries, Kim and Seo *et al.*[71] later modified the threaded α-CD with acrylates and copolymerized the modified PR with butyl acrylate and PEO diacrylate to provide a hydrophobic SRG electrolyte containing LiTFSI salt and 24% DMSO solvent (Fig. 9d). The hydrophobic SRG electrolyte, exhibiting a high ionic conductivity of 2.8×10^{-3} S cm^{-1} and a Li^+ transfer number of 0.61 at 25 °C, offered high O_2 permeability while effectively repelling water molecules, as indicated by a reduced weight increase when exposed to humid air (Fig. 9e). Both Li||Li symmetric cells and Li||O_2 full cells exhibited excellent cycling stability (Fig. 9f).

Gao and Ding *et al.*[72] also reported an SRG electrolyte based on an α-CD-PEO PR (PEO with $M_n = 4000$ Da and 35 threaded α-CDs) crosslinked by a PEO ($M_n = 2000$ Da) macrolinker. By optimizing the PR and PEO crosslinker composition, an SRG electrolyte containing 1 mol L^{-1} LiTFSI in a 1 : 1 (volume ratio) mixture of 1,2-dimethoxyethane (DME) and 1,3-dioxolane (DOL), with 1% $LiNO_3$, achieved an ionic conductivity of 1.73×10^{-3} and a Li^+ transfer number of 0.71 at 30 °C. Consequently, an assembled LFP||Li coin cell showed long and stable cycling at 0.5–16C rate. Additionally, the excellent mechanical properties of SRG electrolyte—1.15 MPa breaking stress and 971% breaking strain—enabled the fabrication of flexible LFP||Li

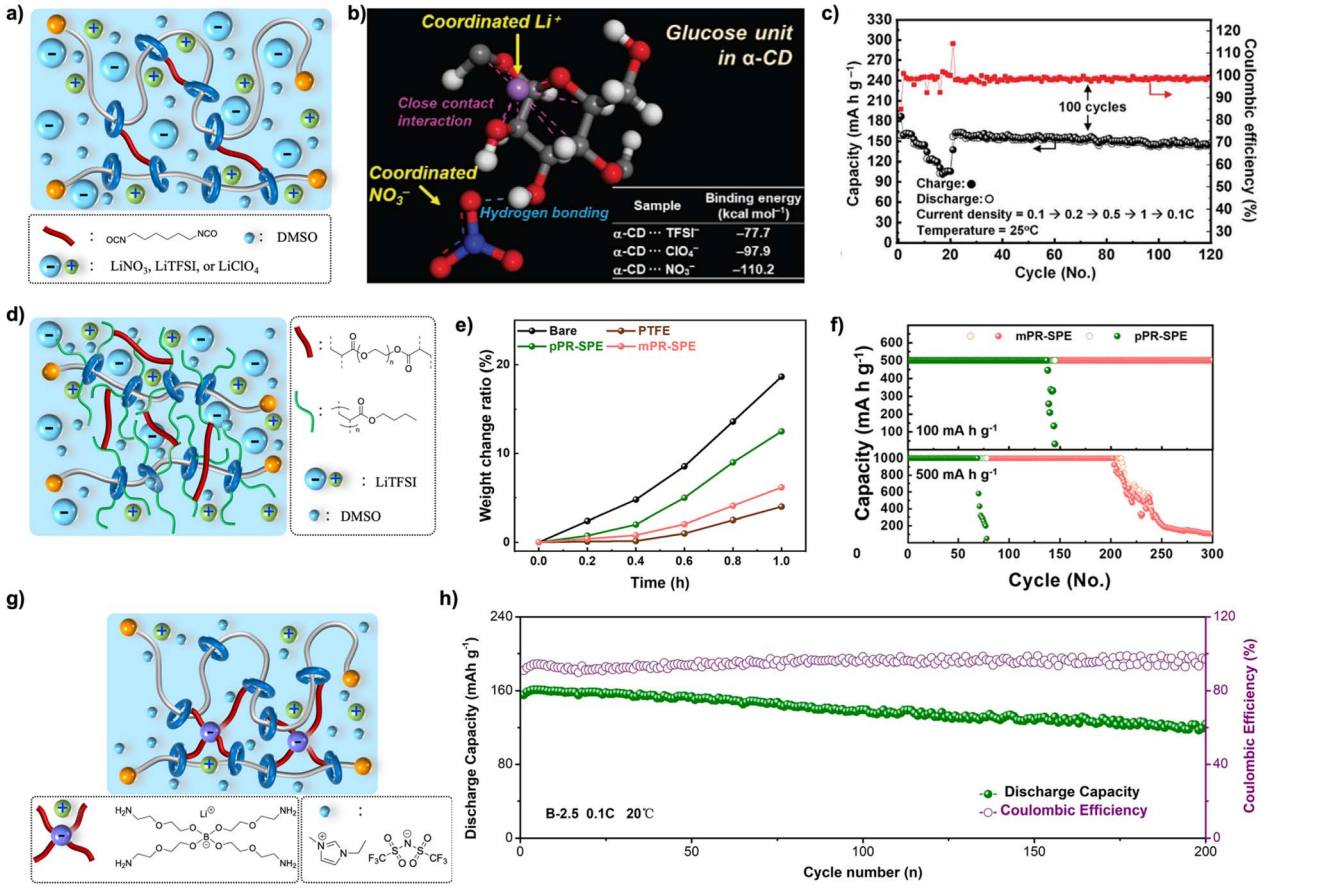

Fig. 9 (a) SRG electrolytes containing different salts. (b) Interaction of α-CD unit with Li^+ cation and various anions in the SRG electrolytes. (c) Performance of a full LFP||Li battery using an SRG electrolyte. (d) An SRG electrolyte containing poly(*n*-butyl acrylate) and PEO diacrylate macrolinker through copolymerization with acrylate-functionalized α-CD (mPR-SPE). (d) The weight change of a bare Li metal, and ones coated with PTFE, SRG electrolyte containing unmodified CD (pPR-SPE) or mPR-SPE. (f) Comparison of a Li||O_2 full battery performance using pPR-SPE and mPR-SPE. (g) An SRG electrolyte crosslinked using a single-ion tetra-arm linker, and (h) its performance in an NMC622||Li full battery. (b and c) are reproduced from ref. 70 with permission from Wiley, copyright 2021, (e and f) are reproduced from ref. 71, and (h) is reproduced from ref. 73 with permission from Wiley, copyright 2021.

pouch cells that underwent stable cycling for 220 cycles at 0.5C while exhibiting resilience to bending and cutting.

More recently, Gohy and Jia *et al.*[73] developed a dynamic SRG electrolyte containing an α-CD-PEO PR (PEO with M_w = 35 000 Da and 100 threaded α-CDs), a tetra-arm boronated single-ion dynamic crosslinker, and 1-ethyl-3-methylimidazolium bis(trifluoromethylsulfonyl)imide (EMIMTFSI)/LiTFSI ionic liquid (Fig. 9g). By fine-tuning the molar ratio of ionic liquid to dynamic crosslinker, they reported an optimized ionic conductivity of 2.21×10^{-3} S cm^{-1} with a Li^+ transfer number of 0.45 at 20 °C. This SRG electrolyte showed thermal stability up to 300 °C and supported stable cycling of a Li‖Li symmetric cells and an NMC622‖Li full cell at 20 °C (Fig. 9h).

3. MIPs as electrode binders

Electrode binder, which typically constitutes 2–30 wt% of the electrode materials depending on the electrode type, provides adhesion between active electrode particles, conductive additives, and the current collector, and also plays crucial roles in the electrochemical redox processes.[74–77] However, the use of MIPs as electrode binders has been less explored compared to their use as electrolytes.

The pioneering work on MIP binders was reported by Choi and Coskun *et al.* in 2017.[27] They aimed to leverage the excellent mechanical adaptability of SRMs to tackle the pulverization challenges of high-energy-density Si anodes, which undergo large volume change (300–400%) during the charging/discharging cycles (Fig. 10a). An α-CD-PEO PR (PEO with M_w = ~20 000 Da and hydroxypropyl α-CDs) was used to crosslink poly(acrylic acid) (PAA, M_w = 450 000 Da), yielding a partially crosslinked SRM that was soluble and amendable to wet electrode processing. The SRM showed a tenfold improvement in mechanical ductility (390% *vs.* 37% rupture strain) compared with the pure PPA polymer. Subsequent electrode fabrication employing Si microparticle, SRM, and super P in a mass ratio of 8 : 1 : 1 yielded a Si anode with an areal loading of ~1 mg cm^{-2}. A fabricated half-cell (2.67 mAh cm^{-2}) with Li as the counter electrode achieved 91% capacity retention after 150 cycles at 0.64 mA cm^{-2} (0.2C). By contrast, a PAA binder afforded only 48% capacity retention after 50 cycles. Further testing of a full battery paring a lithium nickel cobalt aluminium oxides (NCA) cathode (2.88 mA cm^{-2}) at a negative-to-positive electrode capacity ratio (N/P) of 1.15 demonstrated 98% capacity retention after 50 cycles at 0.62 mA cm^{-2} (0.2C), with an average CE of 99.92%. Post-cycling analysis of Si anode revealed less pulverization and a thinner residual SEI layer than the PAA counterpart (Fig. 10b). Choi and Coskun, together with Char *et al.*[78] later adapted this SRM electrode binder to a commercial carbon-coated silicon monoxide (c-SO_x, $x \sim 1$) electrode, which typically presents poor interaction with conventional polar polymer binders. Through strong π–π stacking, c-SO_x was blended with a hydroxylated pyrene, whose hydrogen bonding interaction with PAA facilitated dispersion and fabrication of this commercial c-SO_x electrode material (2.3–2.5 mg cm^{-2}). Full cells in pairing with NCA cathodes (N/P = 1.1) retained 82.5% capacity after 150 cycles at 0.5C (19.4 mg cm^{-2} NCA), and 77.7% capacity after 60 cycles at 0.5C (27.8 mg per cm^2 NCA).

In a similar attempt to address the pulverization challenges of Si anodes, Liang, Yan and Yue *et al.*[79] reported a MIP binder that combines a PAA and an [*an*]daisy chain-based MIP. The MIP was prepared by preforming the [*an*]daisy chain followed by attachment of a supramolecular crosslinking unit containing quadruple hydrogen bonding. Blended with PAA at 5 wt%, this MIP binder, combined with Super P and Si particles, was used to fabricate the electrodes (mass ratio of 1 : 2 : 7) (Fig. 10c). Compared to PAA along or a non-interlocked [*an*]daisy chain, the MIP binder improved electrode adhesion and mechanical resilience. Its use in a Si half-cell (1.1 mg cm^{-2} Si loading) demonstrated 72% capability retention after 300 cycles at 0.5C, with remaining capacity exceeding 1543 mAh g^{-1}, substantially outperforming controls. Full cells pairing an NCM88 cathode (20 mg cm^{-2}) and a prelithiated Si anode (N/P = 1.1) showed 79.2% capacity retention after 100 cycles at 0.2C; and 87% capacity retention after 200 cycles when a prelithiated Si@Gr anode material was used. In a practical demonstration, a 100 mAh NMC811‖Si pouch cell with this MIP binder achieved 80.4% capacity retention after 100 cycles at 0.5C (Fig. 10d).

MIPs were also explored as binders for LFP electrode materials. To address the low ionic conductivity in conventional PVDF binder, Wang and Wang *et al.*[80] designed a composite PR binder containing β-CD-PEO (PEO M_w = 600 000 Da) PR, PVDF (M_w = 100 000 Da), and LiTFSI salt (Fig. 10e). Blending this MIP binder with Super P and LFP in a mass ratio of 1 : 1 : 8 provided LFP electrode with an areal loading of 1.6–10.6 mg cm^{-2}. When paired with a Li anode, the obtained LFP electrode exhibited an initial capacity of 142 mAh g^{-1} and preserved 87.3% capacity after 400 cycles at 1C. Additionally, a 7.46 mAh pouch cell assembled using this LFP electrode demonstrated 82.9% capacity retention after 250 cycles at 0.2C (Fig. 10f).

4. MIPs as electrode coatings

The presence of a stable and robust SEI is crucial for long and stable battery cycling.[81] Formation of such interphase typically occurs *in situ* during battery operation through electrochemical and/or chemical decomposition of electrolytes. Alternatively, applying an artificial SEI (or electrode coating) in advance can improve battery performance. Various type of polymers, including commercial and synthesized ones, have been applied as electrode coatings. Detailed polymers and associated electrode systems have been comprehensively reviewed elsewhere.[4,5] However, MIP-based electrode coatings have been less documented.

In the last decade, Li-metal anode has been regarded as the holy grail of next-generation high-energy-density electrode materials, with a theoretical specific capacity of 3860 mAh g^{-1}. However, uneven deposition of Li and the consequent generation of dead Li significantly compromise cycling stability. Applying coatings on the Li-metal anode has demonstrated great potential for performance improvement (Fig. 11a). Inspired by this strategy, Guo, Cao and Ye *et al.*[82] first applied an SRM coating composed of a PAA chain (M_w = 450 000 Da)

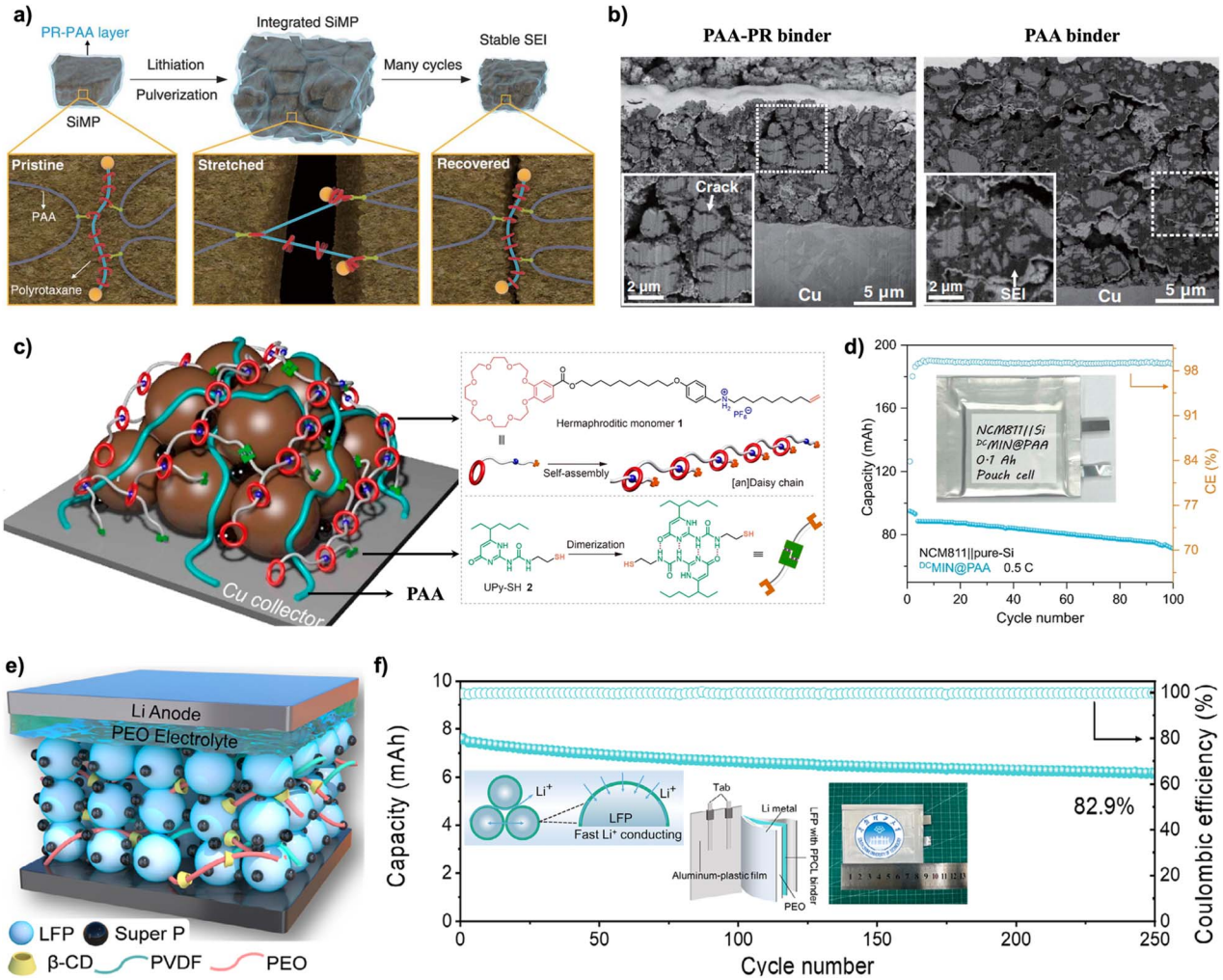

Fig. 10 (a) Mitigation of pulverization in the Si micro-particle (SiMP) anode during the battery cycling through the use of mechanically adaptive PR-PAA binder. (b) Cross-sectional SEM images of SiMP anode after cycling usign PR-PAA and PAA binders (after the 10th delithiation). Si loading, 0.70 mg cm^{-2}; 0.2C rate. (c) Schematic of Si anode material fabricated using a novel MIP binder consisting of supramolecular crosslinked [an] daisy chains, and (d) the cycling performane of a fabricated 100 mAh pouch cell. (e) Illustrated full battery containing hybrid PVDF-PR electrode binder, and (f) corresponding cycling performance of a fabricated pouch cell. The hybrid binder was indicated to facilitate the Li^+ transport at the electrode–electrolyte interface. (a and b) are reproduced from ref. 27, (c and d) are reproduced from ref. 79 with permission from American Chemcial Society, copyright 2024, and (e and f) are reproduced from ref. 80 with permission from Wiley, copyright 2025.

crosslinked by an α-CD-PEO PR (PEO with $M_w = \sim 20\,000$ Da and hydroxypropyl α-CDs), a soluble SRM previously used as binder for Si anode (Fig. 11b). A Li-metal anode with a 10 μm-thick SRM coating exhibited reduced cycling overpotential and dense, even deposition of Li in a Li||Li symmetric cell, contrasting with an uncoated counterpart (Fig. 11c). Consequently, full cells assembled with the SRM-coated Li anode exhibited improved performance compared to non-coated cells. For instance, a full cell pairing an LFP cathode (3 mAh g^{-1}) and a coated Li-metal anode showed an initial capacity of 146 m Ah g^{-1} and retained 83% capacity after 500 cycles at 1C. Increasing the LFP areal loading to >3 mAh cm^{-2} resulted in 94.8% capacity retention after 100 cycles at 0.5C. Similarly, an NMC622 cathode showed an initial capacity of 157 mAh g^{-1} and preserved 80% capacity after 100 cycles at 0.5C (Fig. 11d).

Liang and Yan *et al.*[25] designed a novel MIP coating utilizing a PDMS backbone and a crown ether–ammonium–based rotaxane crosslinker. The crosslinked network coating was generated through a post-photocuring method that enables the use of spin coating for precursor application (Fig. 11e, left). A 100 nm-thick MIP coating enabled dense and even deposition of Li and facilitated stable cycling of a Li||Li symmetric cell for up to 1500 h at 1 mAh g^{-1} (1C). A full cell employing an LFP cathode and a coated Li anode showed an initial capacity of 153 mAh g^{-1} and preserved 88% capacity after 500 cycles at 1C rate (Fig. 11f), outperforming both bare Li anode and a counterpart with covalent network coatings. Later, Liang and Yan, together with Yue *et al.*,[26] designed a novel [*a*n]daisy chain crosslinker for coating formation (Fig. 11e, right). Similarly, this new MIP coating reduced the overpotential in the Li||Li symmetric cells and improved the cycling stability of LFP||Li full cells (Fig. 11g).

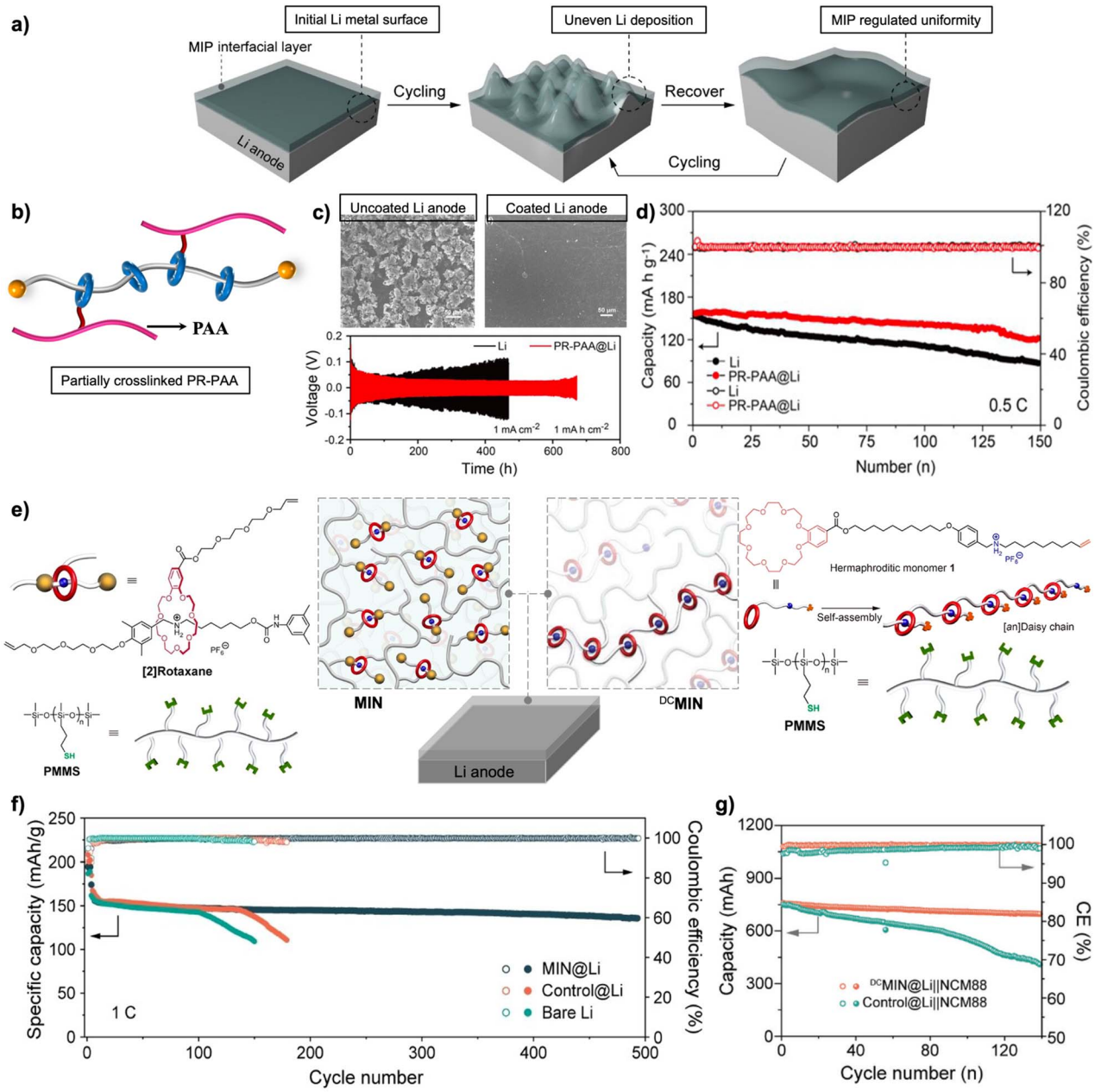

Fig. 11 (a) An MIP coating enabled uniform Li deposition and stable cycling of Li metal anode. (b) Partially crosslinked PR-PAA coating polymer. (c) PR-PAA-coated Li metal anode exhibited more uniform Li deposition and lower overpotential in a Li|Li symmetric cell. (d) A Li-metal anode coated with a PR-PAA polymer showed improved cycling stability compared with a bare one. (e) Two novel MIPs consisting of [2]rotaxane- or [*an*]daisy chain-crosslinked PDMS networks have been applied as Li metal anode coatings, and both exhibited improved capacity retention in (f) a Li||LFP and (g) a Li||NCM88 full battery, respectively. (a) is reproduced from ref. 25 with permission from Wiley, copyright 2022, (c and d) are reproduced from ref. 82 with permission from Wiley, copyright 2023, (e) is reproduced from ref. 25 and 26 with permission from Wiley, copyrights 2022 and 2024, respectively. (f and g) are reproduced from ref. 25 and 26 with permission from Wiley, copyrights 2022 and 2024, respectively.

5. Discussion and outlook

The application of emerging MIPs in batteries has demonstrated significant potential and opened new opportunities for enhancing battery performance. Beyond the specific examples reviewed above, MIPs can be employed across a diverse set of electrochemical systems, including but not limited to high-voltage cathodes,[83] sodium- and zinc-based electrodes,[84] and Li–sulfur batteries.[85] Nevertheless, several challenges must be acknowledged and addressed.

Primarily, this relatively unexplored field–compared to the application of conventional polymer materials – is limited by the synthetic challenges associated with MIPs. Advances in the design and scalable synthesis are essential for their applications

in batteries, especially as polymer electrolytes and electrode binders. For electrode coatings, the required thickness of polymer coating typically ranges from 10 nm to 10 μm,[86,87] thus requiring much less materials in these applications.

Second, the integration of MIPs into batteries depends strongly on their topology. Linear or partially crosslinked MIPs with good solubility in solvents can be processed using conventional solution-based fabrication methods, enabling precise control over composition and coating or binder thickness, and resulting in well-defined interfacial contact. By contrast, processing crosslinked MIPs presents challenges once the networks forms. In particular, an *in situ* or post-fabrication network curing process is necessary to ensure successful integration of crosslinked MIPs as binders or coatings. *In situ* network curing methods—where a liquid polymer precursor is polymerized directly on or within the electrode—can substantially improve the interfacial properties between the electrode and electrolyte. This process enables the polymer network to penetrate pores and conform intimately to the electrode surface and active particles, which results in several key benefits including enhanced interfacial contact, low interfacial resistance and stable and uniform SEI formation.[88,89] Direct use of crosslinked MIPs as polymer electrolytes, (or as membranes to insulate anode and cathode) seems to be more straightforward. However, when using crosslinked MIPs as solid-state electrolytes, achieving effective contact between the electrolyte and electrode remains challenging. Strategies such as *in situ* curing and employing MIPs as catholytes and anolytes can help mitigate this challenge.

Improving the ionic conductivity of solid-state polymer electrolytes stands as a long-term challenge, as is the case for MIP solid-state electrolytes. Previous results have demonstrated the potential of achieving relatively high ionic conductivity ($>10^{-4}$ S cm^{-1}) at near room temperature using MIPs,[50,63,64] comparable to the ionic conductivity of typical liquid electrolytes when infiltrated into membranes. However, a deep understanding of how the mechanical bond motif and associated polymer segmental motion affect ion transport is still lacking. On the other hand, in MIP gel electrolytes, the ionic conductivity can be enhanced by increasing the fraction of plasticizer, albeit at the cost of compromised modulus and mechanical strength. Balanced mechanical strength and ionic conductivity is critical for optimal battery performance, yet the detailed mechanisms underpinning their combined effects remain to be fully elucidated. Finally, the electrochemical compatibility of MIP electrolytes with both anode and cathode needs to be considered, and compositions of polymer backbone and mechanical bond should be pre-evaluated when incorporated into the batteries.

When used as electrode binders, MIPs must provide adhesion both between active material particles and to substrate/current collector. Minimizing binder content while maintaining these adhesion functions is ideal to maximize the loading of active materials and the resulting energy density. Similar to MIP electrolytes, the electrochemical compatibility of MIP binders with electrode materials depends on the choice of polymer backbones and mechanical bond motifs and thus requires thorough evaluation. Additionally, binder materials should ideally swell but not dissolve in liquid electrolytes, especially for the linear or partially crosslinked MIP binders.

MIP coatings for electrodes should also exhibit electrochemically compatibility and remain insoluble in liquid electrolytes. Some studies have indicate that coatings can be ionphilic but solvent-phobic,[90] thereby facilitating ion transfer while mitigating parasitic solvent decomposition at the electrode interface. While MIP coatings have primarily been applied to Li-metal anodes as artificial SEIs, their application as cathode–electrolyte interphases (CEIs)[91] shares some similarities.

To conclude, despite challenges in their designing and synthesis, MIPs have demonstrated great potential for enhancing battery performance through their roles as polymer electrolytes, electrode binders, and coatings.

Conflicts of interest

There are no conflicts to declare.

Data availability

All data discussed in this review are taken from previously published sources, which are appropriately cited in the article.

Acknowledgements

This study is supported by startup grant offered by the Chemistry Department at the University of Waterloo, funding from the Canada Foundation for Innovation (CFI), and funding from the Natural Sciences and Engineering Research Council of Canada (NSERC).

References

1 A. Manthiram, *ACS Cent. Sci.*, 2017, **3**, 1063–1069.
2 J. Lopez, D. G. Mackanic, Y. Cui and Z. Bao, *Nat. Rev. Mater.*, 2019, **4**, 312–330.
3 D. Mecerreyes, N. Casado, I. Villaluenga and M. Forsyth, *Macromolecules*, 2024, **57**, 3013–3025.
4 Z. Yu, Y. Cui and Z. Bao, *Cell Rep. Phys. Sci.*, 2020, **1**, 100119.
5 Z. Huang, H. Lyu, L. C. Greenburg, Y. Cui and Z. Bao, *Nat. Energy*, 2025, **10**, 811–823.
6 X. Zhang, J.-C. Daigle and K. Zaghib, *Materials*, 2020, **13**, 2488.
7 Z. Song, F. Chen, M. Martinez-Ibañez, W. Feng, M. Forsyth, Z. Zhou, M. Armand and H. Zhang, *Nat. Commun.*, 2023, **14**, 4884.
8 F. Zou and A. Manthiram, *Adv. Energy Mater.*, 2020, **10**, 2002508.
9 Y. Shi, X. Zhou and G. Yu, *Acc. Chem. Res.*, 2017, **50**, 2642–2652.
10 H. Yuan, J.-Q. Huang, H.-J. Peng, M.-M. Titirici, R. Xiang, R. Chen, Q. Liu and Q. Zhang, *Adv. Energy Mater.*, 2018, **8**, 1802107.

11 S. Li, Y.-M. Liu, Y.-C. Zhang, Y. Song, G.-K. Wang, Y.-X. Liu, Z.-G. Wu, B.-H. Zhong, Y.-J. Zhong and X.-D. Guo, *J. Power Sources*, 2021, **485**, 229331.
12 Z. Zhang, J. Zhao and X. Yan, *Acc. Chem. Res.*, 2024, **57**, 992–1006.
13 L. Chen, X. Sheng, G. Li and F. Huang, *Chem. Soc. Rev.*, 2022, **51**, 7046–7065.
14 M. K. Beyer, *J. Chem. Phys.*, 2000, **112**, 7307–7312.
15 B. Lee, Z. Niu and S. L. Craig, *Angew. Chem., Int. Ed.*, 2016, **55**, 13086–13089.
16 G. De Bo, *Chem. Sci.*, 2018, **9**, 15–21.
17 L. F. Hart, J. E. Hertzog, P. M. Rauscher, B. W. Rawe, M. M. Tranquilli and S. J. Rowan, *Nat. Rev. Mater.*, 2021, **6**, 508–530.
18 Y. Noda, Y. Hayashi and K. Ito, *J. Appl. Polym. Sci.*, 2014, **131**, 40509.
19 R. Ikura, Y. Ikemoto, M. Osaki, H. Yamaguchi, A. Harada and Y. Takashima, *Polymer*, 2020, **196**, 122465.
20 D. Aoki and T. Takata, *Polymer*, 2017, **128**, 276–296.
21 L. F. Hart, W. R. Lenart, J. E. Hertzog, J. Oh, W. R. Turner, J. M. Dennis and S. J. Rowan, *J. Am. Chem. Soc.*, 2023, **145**, 12315–12323.
22 N. Sugihara, K. Nishimura, H. Nishino, S. Kanehashi, K. Mayumi, Y. Tominaga, T. Shimomura and K. Ito, *Electrochim. Acta*, 2017, **229**, 166–172.
23 Y.-C. Lin, K. Ito and H. Yokoyama, *Polymer*, 2018, **136**, 121–127.
24 L. Imholt, T. S. Dörr, P. Zhang, L. Ibing, I. Cekic-Laskovic, M. Winter and G. Brunklaus, *J. Power Sources*, 2019, **409**, 148–158.
25 J. Zhao, M. Hong, Z. Ju, X. Yan, Y. Gai and Z. Liang, *Angew. Chem., Int. Ed.*, 2022, **61**, e202214386.
26 Z. Shi, Y. Wang, X. Yue, J. Zhao, M. Fang, J. Liu, Y. Chen, Y. Dong, X. Yan and Z. Liang, *Adv. Mater.*, 2024, **36**, 2401711.
27 S. Choi, T. Kwon, A. Coskun and J. W. Choi, *Science*, 2017, **357**, 279–283.
28 X. Xiong, Y. Chen, Z. Wang, H. Liu, M. Le, C. Lin, G. Wu, L. Wang, X. Shi, Y.-G. Jia and Y. Zhao, *Nat. Commun.*, 2023, **14**, 1331.
29 Y. Jiang, Z. Zhang, Y.-X. Wang, D. Li, C.-T. Coen, E. Hwaun, G. Chen, H.-C. Wu, D. Zhong, S. Niu, W. Wang, A. Saberi, J.-C. Lai, Y. Wu, Y. Wang, A. A. Trotsyuk, K. Y. Loh, C.-C. Shih, W. Xu, K. Liang, K. Zhang, Y. Bai, G. Gurusankar, W. Hu, W. Jia, Z. Cheng, R. H. Dauskardt, G. C. Gurtner, J. B.-H. Tok, K. Deisseroth, I. Soltesz and Z. Bao, *Science*, 2022, **375**, 1411–1417.
30 D. Xia, P. Wang, X. Ji, N. M. Khashab, J. L. Sessler and F. Huang, *Chem. Rev.*, 2020, **120**, 6070–6123.
31 R. P. S, V. Prasannavenkadesan, V. Katiyar and A. S. Achalkumar, *RSC Appl. Polym.*, 2025, **3**, 499–531.
32 C. Y. Son and Z.-G. Wang, *J. Chem. Phys.*, 2020, **153**, 100903.
33 L. Long, S. Wang, M. Xiao and Y. Meng, *J. Mater. Chem. A*, 2016, **4**, 10038–10069.
34 Y. Shao, H. Gudla, J. Mindemark, D. Brandell and C. Zhang, *Acc. Chem. Res.*, 2024, **57**, 1123–1134.
35 H. Gudla, A. Hockmann, D. Brandell and J. Mindemark, *ACS Appl. Polym. Mater.*, 2025, **7**, 4716–4724.
36 S. Mogurampelly, O. Borodin and V. Ganesan, *Annu. Rev. Chem. Biomol. Eng.*, 2016, **7**, 349–371.
37 J. Wang, S. Li, Q. Zhao, C. Song and Z. Xue, *Adv. Funct. Mater.*, 2021, **31**, 2008208.
38 A. J. Tsamopoulos and Z.-G. Wang, *ACS Macro Lett.*, 2024, **13**, 322–327.
39 G. Foran, J. Chidiac, C. St-Antoine, P. Nicolle, L. Caradant, A. Prébé and M. Dollé, *Macromolecules*, 2025, **58**, 6820–6828.
40 N. Molinari, J. P. Mailoa and B. Kozinsky, *Chem. Mater.*, 2018, **30**, 6298–6306.
41 Z. Xue, D. He and X. Xie, *J. Mater. Chem. A*, 2015, **3**, 19218–19253.
42 J. Li, J. Li, L. Wan and Z. Li, *Soft Matter*, 2025, **21**, 3410–3424.
43 J. Feng, L. Wang, Y. Chen, P. Wang, H. Zhang and X. He, *Nano Convergence*, 2021, **8**, 2.
44 M. A. Webb, Y. Jung, D. M. Pesko, B. M. Savoie, U. Yamamoto, G. W. Coates, N. P. Balsara, Z.-G. Wang and T. F. I. Miller, *ACS Cent. Sci.*, 2015, **1**, 198–205.
45 L. Yang, D. Wei, M. Xu, Y. Yao and Q. Chen, *Angew. Chem., Int. Ed.*, 2014, **53**, 3631–3635.
46 L. Yang, X. Fu, T. Chen, L. Pan, P. Ji, Y. Yao and Q. Chen, *Chem.–Eur. J.*, 2015, **21**, 6346–6349.
47 X.-B. Fu, L.-Y. Yang, J.-Q. Ma, G. Yang, Y.-F. Yao and Q. Chen, *Polymer*, 2016, **105**, 310–317.
48 Y. Okumura and K. Ito, *Adv. Mater.*, 2001, **13**, 485–487.
49 K. Hashimoto, T. Shiwaku, H. Aoki, H. Yokoyama, K. Mayumi and K. Ito, *Sci. Adv.*, 2023, **9**, eadi8505.
50 B. Kim, E. Lee and J.-H. Seo, *ACS Macro Lett.*, 2024, 1463–1468.
51 R.-D. Wang, Y.-F. Zhang, X.-L. Han, X.-Y. Fan, J. Tian, Y.-K. Gao, T.-T. You and P.-G. Yin, *ACS Appl. Polym. Mater.*, 2024, **6**, 15124–15135.
52 R.-D. Wang, Y.-F. Zhang, X.-L. Han, Y.-K. Gao, T.-T. You and P.-G. Yin, *Eur. Polym. J.*, 2025, **230**, 113893.
53 W. Xue, F. Ahangaran, H. Wang, P. Theato and Y.-J. Cheng, *Macromol. Rapid Commun.*, 2025, 2500207.
54 S. Sen, S. Malunavar and A. J. Bhattacharyya, *J. Phys. Chem. B*, 2016, **120**, 10153–10161.
55 A. Hosseinioun, P. Nürnberg, M. Schönhoff, D. Diddens and E. Paillard, *RSC Adv.*, 2019, **9**, 27574–27582.
56 N. Sugihara, Y. Tominaga, T. Shimomura and K. Ito, *Electrochim. Acta*, 2015, **169**, 433–439.
57 T. Moriyasu, T. Sakamoto, N. Sugihara, Y. Sasa, Y. Ota, T. Shimomura, Y. Sakai and K. Ito, *Polymer*, 2013, **54**, 1490–1496.
58 H. Nishino, C. Liu, S. Kanehashi, K. Mayumi, Y. Tominaga, T. Shimomura and K. Ito, *Ionics*, 2020, **26**, 255–261.
59 L. Imholt, D. Dong, D. Bedrov, I. Cekic-Laskovic, M. Winter and G. Brunklaus, *ACS Macro Lett.*, 2018, **7**, 881–885.
60 K. Kato, K. Inoue, M. Kudo and K. Ito, *Beilstein J. Org. Chem.*, 2014, **10**, 2573–2579.
61 C. A. Angell, C. Liu and E. Sanchez, *Nature*, 1993, **362**, 137–139.
62 Y. Wang, Z. Li, H. Xu, Q. Wang, W. Peng, S. Chi, C. Wang, J. Wang and Y. Deng, *ACS Appl. Mater. Interfaces*, 2023, **15**, 31552–31560.

63 S. Yan, H. Jia, Y. Li, Z. Chen, R. Lyons, Z. He, Y. Zhang, C. Liu, C.-A. Fustin and J.-F. Gohy, *Chem. Eng. J.*, 2024, **495**, 153874.
64 P. Ding, L. Wu, Z. Lin, C. Lou, M. Tang, X. Guo, H. Guo, Y. Wang and H. Yu, *J. Am. Chem. Soc.*, 2023, **145**, 1548–1556.
65 W. Wang and P. Alexandridis, *Polymers*, 2016, **8**, 387.
66 P. Yao, H. Yu, Z. Ding, Y. Liu, J. Lu, M. Lavorgna, J. Wu and X. Liu, *Front. Chem.*, 2019, **7**, 522.
67 J. Li, Z. Wang, Q. Tong, L. Yang, M. Zhu, H. Lin, F. Gao and J. Weng, *Ionics*, 2022, **28**, 3623–3634.
68 Y. He, Y. Li, Q. Tong, J. Zhang, J. Weng and M. Zhu, *ACS Appl. Mater. Interfaces*, 2021, **13**, 41593–41599.
69 H. Xia, G. Xu, X. Cao, C. Miao, H. Zhang, P. Chen, Y. Zhou, W. Zhang and Z. Sun, *Adv. Mater.*, 2023, **35**, 2301996.
70 J. Seo, G. Lee, J. Hur, M. Sung, J. Seo and D. Kim, *Adv. Energy Mater.*, 2021, **11**, 2102583.
71 B. Kim, M.-C. Sung, G.-H. Lee, B. Hwang, S. Seo, J.-H. Seo and D.-W. Kim, *Nano-Micro Lett.*, 2025, **17**, 31.
72 X. Deng, J. Chen, X. Jia, X. Da, Y. Zhao, Y. Gao, Y. Gao, X. Kong, S. Ding and G. Gao, *Angew. Chem., Int. Ed.*, 2024, e202410818.
73 S. Yan, J. Liu, Z. He, H. Jia, Z. Chen, Y. Zhang and J.-F. Gohy, *Angew. Chem., Int. Ed.*, 2025, **64**, e202503307.
74 S. Bandyopadhyay and B. Nandan, *Energy Storage Mater.*, 2025, **78**, 104233.
75 Y. Ding, Y. Wang, C. Liu, J. Deng, S. Qu, Y. Wang, R. Bai, Y. Liu, G. Liu, C. Yue, W. Yu, Z. Zhang and X. Yan, *Angew. Chem., Int. Ed.*, 2025, **64**, e202510140.
76 D.-Y. Han, I. K. Han, J. Y. Kwon, S. Nam, S. Kim, Y. Song, Y. Kim, Y. S. Kim, S. Park and J. Ryu, *Adv. Sci.*, 2025, **12**, 2417143.
77 J. Kang, J. Kwon, D.-Y. Han, S. Park and J. Ryu, *Appl. Phys. Rev.*, 2024, **11**, 011315.
78 Y. Cho, J. Kim, A. Elabd, S. Choi, K. Park, T. Kwon, J. Lee, K. Char, A. Coskun and J. W. Choi, *Adv. Mater.*, 2019, **31**, 1905048.
79 Z. Liu, Y. Wang, G. Liu, X. Yue, Z. Shi, Y. Tan, J. Zhao, Y. Lei, X. Yan and Z. Liang, *J. Am. Chem. Soc.*, 2024, **146**, 34491–34500.
80 H. Liu, S. Wang, W. Kong, Y. Liu and H. Wang, *Angew. Chem., Int. Ed.*, 2025, **64**, e202507579.
81 H. Adenusi, G. A. Chass, S. Passerini, K. V. Tian and G. Chen, *Adv. Energy Mater.*, 2023, **13**, 2203307.
82 R. Gao, H. Yang, C. Wang, H. Ye, F. Cao and Z. Guo, *Angew. Chem., Int. Ed.*, 2021, **60**, 25508–25513.
83 W. Li, B. Song and A. Manthiram, *Chem. Soc. Rev.*, 2017, **46**, 3006–3059.
84 L. P. Wang, L. Yu, X. Wang, M. Srinivasan and Z. J. Xu, *J. Mater. Chem. A*, 2015, **3**, 9353–9378.
85 L. Tang, H. Peng, J. Kang, H. Chen, M. Zhang, Y. Liu, D. H. Kim, Y. Liu and Z. Lin, *Chem. Soc. Rev.*, 2024, **53**, 4877–4925.
86 J. Lopez, A. Pei, J. Y. Oh, G.-J. N. Wang, Y. Cui and Z. Bao, *J. Am. Chem. Soc.*, 2018, **140**, 11735–11744.
87 S. Stalin, M. Tikekar, P. Biswal, G. Li, H. E. N. Johnson, Y. Deng, Q. Zhao, D. Vu, G. W. Coates and L. A. Archer, *Nano Lett.*, 2020, **20**, 5749–5758.
88 S. Li, H. Gao, J. Tan, Z. Qiu, X. Guo and Y. Yan, *ACS Appl. Mater. Interfaces*, 2025, **17**, 55338–55346.
89 H. Wu, G. Yu, L. Pan, N. Liu, M. T. McDowell, Z. Bao and Y. Cui, *Nat. Commun.*, 2013, **4**, 1943.
90 Z. Huang, J.-C. Lai, S.-L. Liao, Z. Yu, Y. Chen, W. Yu, H. Gong, X. Gao, Y. Yang, J. Qin, Y. Cui and Z. Bao, *Nat. Energy*, 2023, **8**, 577–585.
91 S. P. Kühn, K. Edström, M. Winter and I. Cekic-Laskovic, *Adv. Mater. Interfaces*, 2022, **9**, 2102078.